

ANALYTICAL POTENTIAL OF A SELECTIVELY MODULATED
INTERFEROMETRIC DISPERSIVE SPECTROMETER

By

Thomas Lee Chester

A DISSERTATION PRESENTED TO THE GRADUATE COUNCIL OF
THE UNIVERSITY OF FLORIDA
IN PARTIAL FULFILLMENT OF THE REQUIREMENTS FOR THE
DEGREE OF DOCTOR OF PHILOSOPHY

UNIVERSITY OF FLORIDA

1976

This work is dedicated to Ellen, my wife,
and to Carolyn, my daughter. Their sacri-
fices for this work were much greater than
my own.

ACKNOWLEDGMENTS

The author wishes to acknowledge the support given during his final year at the University of Florida through the Chemistry Departmental Fellowship which was sponsored by the Procter and Gamble Company.

The author is also very grateful for the advice, encouragement and support given by Professor James D. Winefordner and by the numerous members of the JDW group. Their efforts and contributions have led to success for many individuals.

TABLE OF CONTENTS

ACKNOWLEDGMENTS	iii
ABSTRACT	v
CHAPTER	
I INTRODUCTION	1
II THEORY OF SEMIDS	5
The Michelson Interferometer	8
SISAM	18
SEMIDS	27
III THE SEMIDS INSTRUMENT	31
Alignment	31
Modulation	38
Demodulation	69
IV SIGNALS, NOISES AND SIGNAL-TO-NOISE RATIOS IN SPECTROMETRY	73
Signals	75
Noises	80
Noise Sources	87
Signal-to-Noise Ratios	90
Modulation	92
Spectral Bandwidth Considerations	95
V THE SIGNAL-TO-NOISE RATIO FOR SEMIDS	100
Signal	100
Noise	101
Signal-to-Noise Ratio for SEMIDS	108
VI CONCLUSIONS	118
APPENDIX	120
LITERATURE CITED	122
BIOGRAPHICAL SKETCH	126

Abstract of Dissertation Presented to the
Graduate Council of the University of Florida in Partial
Fulfillment of the Requirements for the Degree of
Doctor of Philosophy

ANALYTICAL POTENTIAL OF A SELECTIVELY MODULATED
INTERFEROMETRIC DISPERSIVE SPECTROMETER

By

Thomas Lee Chester

June, 1976

Chairman: James D. Winefordner
Major Department: Chemistry

The Selectively Modulated Interferometric Dispersive Spectrometer (SEMIDS) is a modified version of the Michelson interferometer which is obtained by replacing the stationary mirror with a rotatable diffraction grating. The multiplex signal nature of the Michelson interferometer is eliminated and mechanical tolerance requirements are greatly reduced thus making interferometric spectral measurements in the uv-visible spectral region possible and without the need of a computer. Compared to a conventional dispersive spectrometer using the same grating, SEMIDS provides an increase of 10^2 to 10^3 in the luminosity-resolving power product. This offers a potential signal-to-noise ratio (S/N) improvement capability, which is offset by a potential S/N disadvantage by noise carried on non-dispersed light.

Generation of signals is treated in theory and in practice. Emphasis is placed on alignment requirements and procedures and on signal modulation and demodulation.

A general treatment of S/N theory is presented in adequate detail to develop a S/N expression for SEMIDS. Proportional noises are discussed in detail. Also, a concept of separate spectral bandwidths for signal and noise components is introduced.

A general S/N model is derived for SEMIDS. The model properly describes SEMIDS' performance in measuring flame atomic emission. The S/N model is compared to a similar model for a conventional spectrometer. From this comparison, the applications of potential usefulness of SEMIDS are predicted.

SEMIDS' greatest analytical usefulness is concluded to be for measurements in the infrared spectral region where the use of the instrument will be a reasonable compromise between conventional spectrometry and Fourier Transform Spectrometry.

CHAPTER I INTRODUCTION

Spectrometric measurement methods can be divided into two categories. The first contains the more conventional methods which involve either spectral dispersion or some other form of spatial separation of the light components. Then each component is measured separately from the others, usually in a sequential manner with a single detector. Colorimeters and prism and grating spectrometers belong to this category. The second category contains the less conventional multiplex methods. In these methods, the radiation is not (necessarily) spectrally dispersed, but rather, the spectral components are encoded by a signal modulation scheme. Each spectral component gives rise to a unique modulation function which distinguishes it from the others and allows for its measurement in the presence of others. Thus, all of the spectral signals may be measured all of the time by a single detector. The Michelson interferometer,¹⁻⁷ the Hadamard spectrometer,⁸⁻¹¹ the Mock interferometer,¹² and the Non-dispersive Atomic Fluorescence spectrometer^{13,14} are examples of multiplex methods.

Since all spectral components are measured simultaneously in multiplex methods, a substantial increase in the information

gathering efficiency results. In addition, the light gathering power or luminosity of multiplex based spectral instruments is, in general, higher than that of conventional dispersive spectrometers by two or three orders of magnitude. This also gives rise to another substantial improvement in information gathering efficiency when compared to conventional dispersive spectrometers. These efficiency improvements lead to higher signal levels and higher noise levels. However, if the signal level increase is greater than the increase in the noise level, an overall gain in the signal-to-noise ratio (S/N) is accomplished (see Chapter IV). It is the existence of such a S/N improvement in many measurement situations that justifies the further investigation of multiplex methods.

When a Michelson interferometer is used in spectrometry, it is most often called a Fourier Transform Spectrometer, the name by which it is known commercially. It has received increasing popularity in recent years due to its exceptional performance in the infrared spectral region. S/N improvements as high as three orders of magnitude have been reported in addition to a substantial improvement in resolving power as compared to conventional dispersive spectrometers.¹⁵ However, the use of the Michelson interferometer has been mostly limited to the infrared spectral region by the requirement that mechanical tolerances be maintained to a small fraction of the shortest wavelength to be measured. Even in the infrared region, it is now a common practice to monitor the

measuring interferometer with a reference interferometer to insure that tolerances are maintained during operation. A second difficulty in the general use of the Michelson interferometer (or any multiplex technique) is that the spectrum cannot be recorded directly due to the multiplex nature of the spectral signals. The signal which is recorded is the summation of the separate signals of each spectral component and must be de-multiplexed (decoded) to yield the spectral information. Thus, signal processing is a serious (and expensive) problem facing the use of multiplex instrumentation. (However, this problem is continuously diminishing with the almost daily advances of digital electronics. At the time of this writing, dedicated minicomputers are commonly incorporated with Fourier Transform Spectrometers and thus are a large fraction of the cost of the complete instrument. It is reasonable to expect that the next generation of Fourier Transform Spectrometers will employ microprocessors at a substantial cost reduction. Future developments will lead to even lower costs.)

The Selectively Modulated Interferometric Dispersive Spectrometer (SEMIDS) was designed to circumvent both of these problems and permit interferometric measurements to be easily made in the uv-visible spectral region. Unfortunately, to accomplish this, signal multiplexing had to be eliminated. The result is a hybrid instrument which gives single component signals but employs interferometric optics and achieves a substantial luminosity increase over that of

a conventional dispersive spectrometer used at the same resolving power. It was hoped that this luminosity advantage would result in improvements in the S/N for analytical measurements in the uv-visible spectral region. Mechanical tolerances have been greatly reduced and no computer is required for signal processing.

SEMIDS was expected to give S/N improvements in spectral measurements which are usually limited by the amount of available light. Thus, it was felt that limits of detection could be improved in flame atomic emission and fluorescence and in molecular fluorescence.

The failure of SEMIDS to perform even comparably with conventional spectrometry in the first application attempted, flame atomic emission, led to the S/N characterization which is presented here. The purpose of this characterization was first to discover exactly why SEMIDS failed and, second to predict what measurements, if any, could be improved with the use of SEMIDS.

CHAPTER II THEORY OF SEMIDS

The theory of the Selectively Modulated Interferometric Dispersive Spectrometer (SEMIDS) proceeds most logically in nearly chronological order. Let us begin with a brief discussion of interference.

Interference is defined as the superposing of separate wave displacements to arrive at a resultant wave displacement.¹⁶ If the resultant displacement is larger than both of the separate wave displacements, the interference is said to be constructive, while if the resultant displacement is smaller than either of the separate displacements the interference is called destructive. In order for interference to result in a stable pattern, the sources of the separate waves must be coherent; that is, there must exist a point to point phase relationship between the two sources which is fixed in time.¹⁷ In dealing with light waves, there are two fundamental methods for obtaining coherence between two light sources. The first of these is known as division of wave front in which a wave front is divided laterally without a loss in amplitude. This is best illustrated by Young's experiment (Figure 1). Huygen's Principle states that any point on a wave front can be considered as a new source of

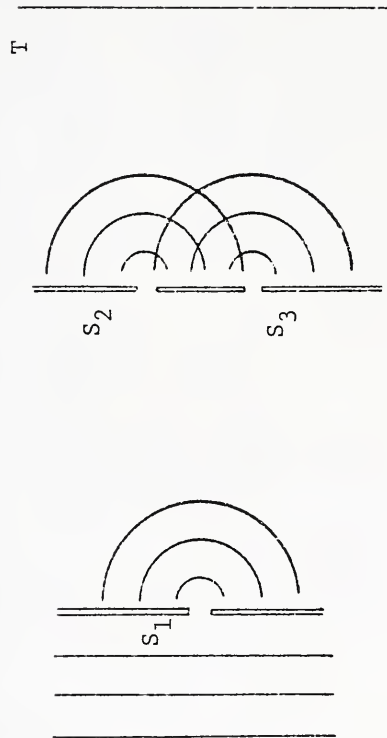


Figure 1. Interference by division of wave front.
Young's Experiment.

waves. This is the basis of diffraction which is the bending of waves around an obstacle. Thus, plane waves (perhaps produced from a small source placed a large distance away) falling on the first slit, S_1 , are diffracted and result in the generation of cylindrical waves. The two slits, S_2 and S_3 , are placed equidistant from S_1 , thus each wave front reaches these two slits simultaneously. Diffraction occurs again at both S_2 and S_3 resulting in two cylindrical wave fronts. However, since each of these was derived from a common wave, a phase relationship must exist. Thus S_2 and S_3 are coherent sources, and interference of their wave fronts results in a standing interference pattern which may be observed by viewing the target, T.

Coherence may also be produced by division of amplitude, in which a wave is divided across its width by a partially reflecting mirror. Interference by division of amplitude is the reason for the existence of multicolored patterns on soap bubbles and oil slicks when viewed with white light.

Two interferometric instruments commonly used in spectrometry are the Fabry-Perot and the Michelson interferometers. Both of these employ division of amplitude. A discussion of the Fabry-Perot is not pertinent to the chronology leading to SEMIDS, and the interested reader is referred to other works.^{18,19}

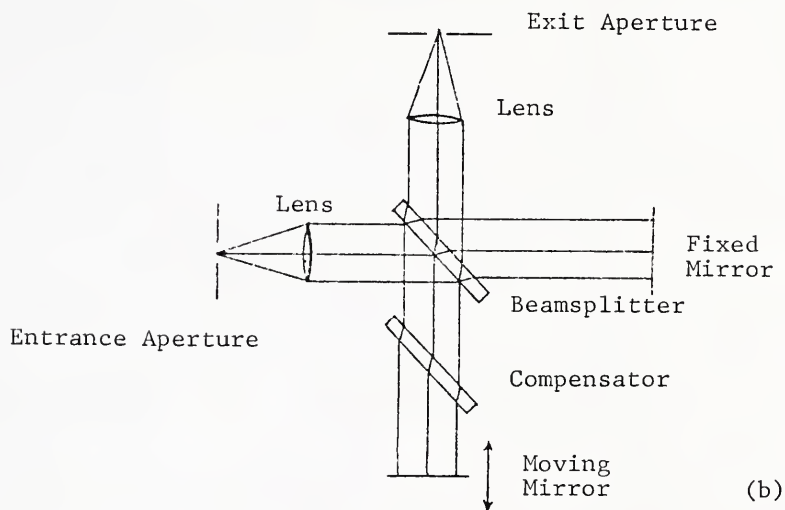
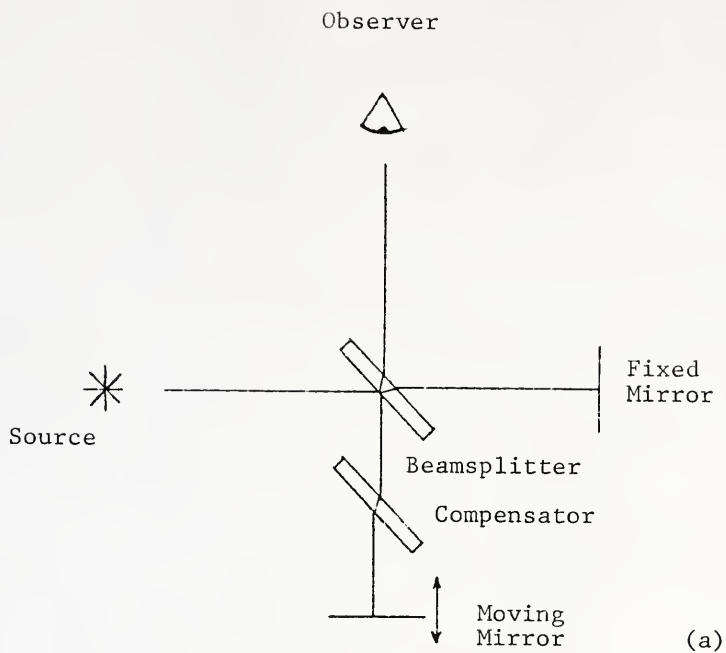
The Michelson Interferometer

The Michelson interferometer was discussed briefly in the Introduction. The basic Michelson interferometer is illustrated in Figure 2. A ray is divided by the beamsplitter into two rays - one transmitted and one reflected. Each ray is reflected by a plane mirror and returned to the beamsplitter where each is again divided. The two sets of two rays, each ray having $1/4$ the intensity of the original, exit the instrument; one pair toward the source and the other pair along the fourth arm. Interference occurs between the two rays in each exiting pair. Concentric circular interference fringes will be produced for monochromatic light when the reflecting mirrors are precisely set at equal inclination angles with respect to the axis on which each is located. The number of fringes observed depends on the optical path difference between the two arms and on the wavelength of the light. The optical path length of each arm is the summation of the products of the geometric path length and the refractive index of each material through which the light must pass:

$$l_o = \sum_i l_i \mu_i \quad (1)$$

where l_i is the geometric path length in species i of refractive index μ_i and l_o is the optical path length. The optical path difference is computed for any two rays derived from the same parent ray and is constant over the entire cross section of the instrument only when the mirrors are at equal inclination angles and only for one value of the geometric

Figure 2. (a) The basic Michelson interferometer.
(b) The modified version used in spectrometry.



path difference, i.e., the one yielding an optical path difference equal to zero. For these conditions, the entire exit plane is filled with a single fringe, i.e., a field of uniform tint is produced. If the path difference is now changed in either direction by translating one of the mirrors along its axis, the interference pattern will collapse to the center as rings are formed at the edge of the field. As the path difference is increased, rings will be formed at the edge faster than they move to the center and disappear. Thus, the total number of rings observed depends on the optical path difference.

Because the refractive index of all materials is a function of wavelength, zero optical path difference can only occur for one wavelength at a time unless the geometric paths through each material are identical in both arms of the interferometer. To accomplish this, the beamsplitter must be optically symmetric. Beamsplitters are chosen for specific spectral regions and are only several wavelengths in thickness. Thus (especially in the uv-visible spectral region) another physical support is often necessary. When the beamsplitter is supported by a single glass plate, a compensating plate of the same material and dimensions is placed parallel to the first in the reflecting arm facing the active surface of the beamsplitter plate. Thus, each ray must make two full passes through the beamsplitter substrate between the occurrences of division and recombination of the rays.

In spectrometry, the measurement of the wave intensity (which equals the square of the wave amplitude) of particular wavelength components is sought. Because the interference for the j th wavelength component changes from constructive to destructive for each incremental change in the (round trip) path difference of $\lambda_j/2$, the wavelength components may be sorted by changing the optical path difference in a linear fashion, i.e., by translating one mirror along its axis at a constant velocity. Thus the amplitudes of the modulation frequencies produced are indicative of the intensity of each spectral component because

$$f_j = 2v/\lambda_j, \quad (2)$$

where f_j , Hz, is the modulation frequency of the λ_j , m, spectral component and v , m s^{-1} , is the mirror velocity. All real measurements are made in the time domain. In conventional scanning spectrometry, the wavelength detected varies linearly with time, and the spectrum is recorded directly. However, with the Michelson interferometer, this wavelength-time relationship does not exist. The wavelength information exists in the frequency domain as is evident from Equation 2. Thus, the signal recorded in the time domain must be transformed to the frequency domain in order for the spectral information to be recovered. This is accomplished by a Fourier Transform and is the root of the name Fourier Transform Spectrometry.

To make such measurements with a simple Michelson interferometer, an aperture must be placed in the exit arm which

just passes the smallest center fringe formed during the experiment. This fringe will be formed for the shortest wavelength at the maximum path difference. The aperture is necessary to insure that the detected radiation has maximum contrast between constructive and destructive interference. As a result, only a small fraction of the light collected from the source may actually reach the detector.

If a field of uniform tint can be maintained for all values of the path difference, then all of the collected radiation can be detected. This was first accomplished by Twyman and Green who used a small entrance aperture coupled with a collimating lens to produce plane waves which are perpendicular to the optical axis (Figure 2b).³ Since, at any point in time, the phase relationship of the waves is fixed over the cross section of any arm of the interferometer, a field of uniform tint must result for all values of the path difference. The entire exit beam may be focused on the detector.

"Perfect" plane waves are only produced by a collimator viewing a point source. Point sources are not practical in the real sense, and so it is important to know how large the aperture can be made before serious deviation from the field of uniform tint is encountered. This is also related to the maximum optical path difference to be encountered (which may be obvious since any wave front produces a field of uniform tint at zero optical path difference). The maximum solid angle, Ω_M , sr, which may be subtended by the aperture

at the collimator, is given by²⁰

$$\Omega_M = \frac{2\pi}{R} , \quad (3)$$

where R is the resolving power, $R = \lambda/\Delta\lambda$, which is desired and is given by²¹

$$R = X_m/\lambda \quad (4)$$

for the Michelson interferometer. X_m , m, is the maximum optical path difference to be encountered. It is curious to note from Equation 4 that the greatest resolving power, R_{\max} , is attained for the shortest wavelength, λ_s , for a given value of X_m .

The solid angle can be expressed geometrically approximately by

$$\Omega = \frac{\pi r^2}{f^2} , \quad (5)$$

where r is the radius of the aperture and f is the focal length of the collimator. Equating Equation 3 with Equation 5, the maximum allowed radius of the aperture is found to be

$$r_{\max} = f\sqrt{\frac{2\lambda_s}{X_m}} \quad (6)$$

or

$$r_{\max} = f\sqrt{\frac{2}{R_{\max}}} . \quad (7)$$

In practice, it is more common to accurately position the moving mirror at a series of fixed locations rather than by moving it at a constant velocity. This is more conducive to sampling by an analog-to-digital converter for subsequent digital Fourier Transformation. Thus, a plot of detector

current vs. the optical path difference is called an interferogram. The cosine Fourier Transform of the interferogram is the spectrum.

Sampling of the interferogram at various values of the optical path difference is critical in terms of the desired resolution and the spectral range to be covered. These conditions do not exist in SEMIDS, and the interested reader is referred to an excellent discussion by Bell.²² The true underlying restrictions are due to the nature of the Fourier Transform and are explained in another reference.²³

The light intensity impinging upon the detector can be derived as follows. For each spectral component, λ_j , the intensity of the light collected and collimated is I_j and has a wave amplitude A_j . This intensity is split by the beamsplitter, and the two beams formed each have intensity $I_j/2$ and amplitude $A_j/\sqrt{2}$ assuming a perfect beamsplitter with 50% reflection and 50% transmission is used. Each beam will undergo a phase change associated with transmission or reflection. This is most easily expressed by writing the wave amplitude in complex form as $A \exp(i\theta)$ where A is the amplitude, θ is the phase angle and $i = \sqrt{-1}$. Thus we have

$$\frac{A_j}{\sqrt{2}} \exp(i\theta_{TB}) \quad \text{and} \quad \frac{A_j}{\sqrt{2}} \exp(i\theta_{RB})$$

as the complex amplitudes of the two beams where θ_{TB} and θ_{RB} are the phase changes incurred by transmission and reflection at the beamsplitter, respectively. Each beam is now reflected by a plane mirror and returned to the beamsplitter. The com-

plex amplitudes of the beams at the beamsplitter, but just prior to interaction with it, are

$$\frac{A_j}{\sqrt{2}} \exp (i\theta_{TB} + 2\pi id_1/\lambda_j + i\theta_{RM}) \quad (8)$$

and

$$\frac{A_j}{\sqrt{2}} \exp (i\theta_{RB} + 2\pi id_2/\lambda_j + i\theta_{RM}) , \quad (9)$$

where d_1 and d_2 are the optical path lengths of the reflecting arms for a round trip and θ_{RM} is the phase change due to reflection from a plane mirror which is assumed to be the same for each arm if the mirrors are identical and are equally inclined. Each beam is now split again by the beamsplitter. For the resultant beams entering the fourth arm of the interferometer, the complementary beamsplitter interaction occurs, i.e., the previously transmitted beam is now reflected and vice versa. The intensity of each beam is also again divided by 2 and the amplitude divided by $\sqrt{2}$. Thus, two beams, each of intensity $I/4$ and complex amplitudes

$$\frac{A_j}{\sqrt{2}} \exp (i\theta_{TB} + 2\pi id_1/\lambda_j + i\theta_{RM} + i\theta_{RB}) \quad (10)$$

and

$$\frac{A_j}{\sqrt{2}} \exp (i\theta_{RB} + 2\pi id_2/\lambda_j + i\theta_{RM} + i\theta_{TB}) \quad (11)$$

exit the fourth arm and interfere. The amplitude of the resultant wave is found by adding the complex amplitudes of the interfering waves. This is

$$\frac{A_j}{\sqrt{2}} \exp (i\theta_{TB} + i\theta_{RB} + i\theta_{RM}) [\exp (2\pi id_1/\lambda_j) + \exp (2\pi id_2/\lambda_j)] . \quad (12)$$

The resultant intensity, $I_j(\Delta)$, is obtained by multiplying this amplitude by its complex conjugate:

$$I_j(\Delta) = \frac{A_j^2}{4} [2 + \exp(2\pi i d_1/\lambda_j - 2\pi i d_2/\lambda_j) + \exp(-2\pi i d_1/\lambda_j + 2\pi i d_2/\lambda_j)] \quad (13)$$

Substitution of the identity

$$\exp(\pm i\theta) = \cos \theta \pm i \sin \theta$$

results in elimination of the imaginary terms, and the result is

$$I_j(\Delta) = \frac{A_j^2}{2} [1 + \cos(2\pi\Delta/\lambda_j)], \quad (14)$$

where Δ is the optical path difference, $d_1 - d_2$.

Since it is the time averaged intensity which is measured by the detector rather than the instantaneous intensity due to the superposition of waves of many wavelengths, it is sufficient to integrate Equation 14 over all wavelengths to obtain the total intensity as a function of Δ ,

$$I(\Delta) = \int_{\lambda_\ell}^{\lambda_u} \frac{A(\lambda)^2}{2} [1 + \cos(2\pi\Delta/\lambda)] d\lambda, \quad (15)$$

where λ_ℓ and λ_u are the lower and upper wavelength limits of the spectrum, respectively, which are determined by the transmission of the optical components and the spectral response of the detector. For a spectrum consisting of lines which are narrower than the resolution intervals of the interferometer, it is sufficient to simply sum the line intensities:

$$I(\Delta) = \sum_{j=1}^L \frac{A_j^2}{2} [1 + \cos(2\pi\Delta/\lambda_j)]. \quad (16)$$

This summation is easier to comprehend than the integral above, and it will be used later.

It is not totally correct to assume that θ_{RB} is the same for both beams. Since the reflections occur from opposite sides of the beamsplitter, any asymmetry in its construction could cause the phase changes to be different. If the beamsplitter is a coated flat plate, then one reflection occurs from the air side and the other from the substrate side which clearly can not result in the same phase change. At worst, a phase offset should be added to the argument of the cosine in Equations 15 and 16.

SISAM

There are two main difficulties confronting the use of a Michelson interferometer for spectrometry. The first is the necessity of performing a Fourier transform to recover the spectral information. This can be accomplished either by digital techniques or by a hard-wired frequency spectrum analyzer. Both are expensive and are unnecessary in conventional spectrometry. Additionally, a large number of points must be sampled in the uv-visible spectral region (compared to the infrared) in order for Fourier Transform Spectrometry to achieve the free spectral range of conventional dispersive spectrometry without undersampling the interferogram. This adds to the complexity and expense of performing the Fourier transform. Undersampling leads to spectral confusion by aliasing which is the inability to

distinguish a frequency from its undertones.

The second difficulty is the requirement of knowing the optical path difference to an accuracy of small fractions of the shortest wavelength to be measured. This has restricted the use of Fourier Transform Spectrometry to wavelengths in the infrared region and longer for the most part.

Both of these difficulties are eliminated (but, unfortunately, a third is generated) by a modification of the Michelson interferometer first described by Connes which he called SISAM (spectromètre interférentiel à sélection par l'amplitude de modulation).²⁴ Subsequently, many publications have appeared by a variety of workers.²⁵⁻⁴¹ This instrument (Figure 3) is basically a Michelson interferometer in which both plane mirrors are replaced with identical diffraction gratings which are carefully adjusted to the same angle. Fringes of equal inclination are produced only for the single wavelength which solves the grating equation for the Littrow configuration. That wavelength is the one for which rays are returned on their original paths. For all other wavelengths, the gratings appear to be set at equal but opposite inclination angles. If the optical path difference is changed linearly with time, modulation occurs as in the Michelson interferometer except that the modulation depth is now selected by the choice of the Littrow wavelength, i.e., by the tilt of the gratings. The modulation depth, M , which is the difference between maximum and minimum observed intensities divided by the maximum observed in-

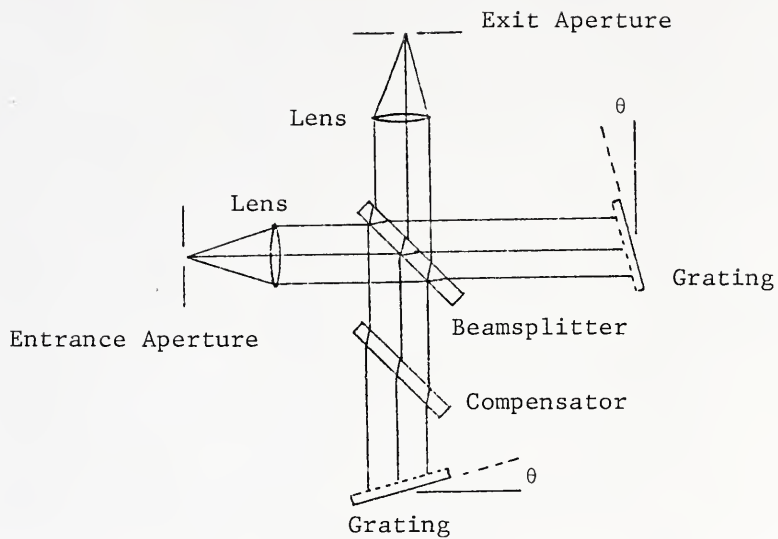


Figure 3. The SISAM spectrometer.

tensity, can be given as a function of wavenumber or wavelength by

$$M = \text{sinc } 2\pi[(\sigma - \sigma_0) W \tan \theta] \quad (17)$$

or

$$M = \text{sinc } 2\pi\left[\left(\frac{1}{\lambda} - \frac{1}{\lambda_0}\right) W \tan \theta\right], \quad (18)$$

where σ_0 and λ_0 are the Littrow wavenumber and wavelength for the grating angle θ and W is the width of the flux assuming the gratings are the limiting field stops. The sinc function* is defined as $\text{sinc } \theta = (\sin \theta)/\theta$ and may possess negative values. The existence of a negative modulation depth for wavelength λ_j implies a π phase change in the modulated signal for that wavelength compared to the signal for the Littrow wavelength, λ_0 . The sinc function is plotted in Figure 4a. It can be seen that M decreases rapidly for wavelengths different from λ_0 . The Rayleigh criterion is used to define resolution, i.e., the two wavelengths will be resolved when the peak of one coincides with the first zero of the other. The first zero of the sinc function occurs when the argument equals π . Thus, the resolving power may be found by solving

$$2\pi[(\sigma - \sigma_0) W \tan \theta] = \pi \quad (19)$$

* The sinc function has objectionably large side lobes which lead to large secondary maxima in the observed signals. For this reason, it is common to choose another modulation function at the expense of resolving power by a technique known as apodization where the grating behavior is changed by placing a mask over the grating surface (see Figure 4b).

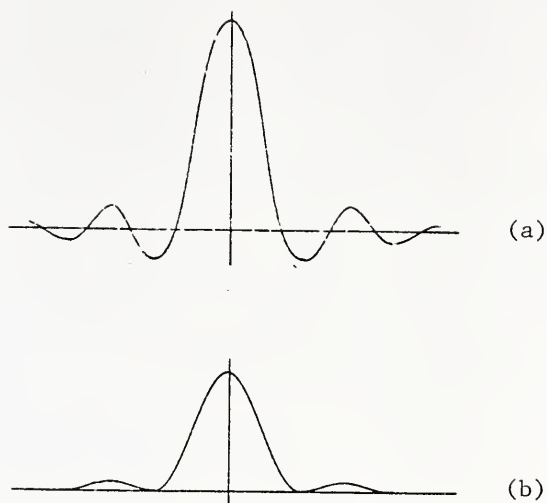


Figure 4. (a) The sinc function, $y = \text{sinc } 2x$.
(b) A function of the form $y = \text{sinc}^2 x$ may be obtained by apodization.

or

$$2(\sigma - \sigma_0) \frac{W}{\cos \theta} \sin \theta = 1. \quad (20)$$

$W/\cos \theta$ is the width of the grating. From the grating equation for the Littrow configuration, $m\lambda = 2d \sin \theta$, $\sin \theta$ is given by $\sin \theta = m/2d \sigma_0$ where m is the diffraction order and d is the distance between adjacent grooves. Because the grating width divided by the groove spacing yields the number of grooves, N ,

$$\frac{(\sigma - \sigma_0)}{\sigma_0} mN = 1 \quad (21)$$

is obtained by substitution. Since $\sigma_0/(\sigma - \sigma_0)$ is the resolving power, R , when σ_0 is just resolved from σ , then

$$R = mN \quad (22)$$

for SISAM. That is, the resolving power equals the theoretical resolving power of the gratings.

As for the Michelson interferometer, the entrance solid angle must be limited to $\Omega_M = 2\pi/R$ for SISAM to operate near the resolving power limit. Because the resolving power is limited by the number of grating grooves rather than by a more easily controllable parameter such as maximum path difference, it is not possible to trade a smaller solid angle for higher resolving power. However, contrary to conventional spectrometers, the resolving power is essentially equal to the theoretical maximum for all values of Ω up to Ω_M . This results in a sizable improvement in luminosity (light gathering power) for SISAM over the conventional spectrometer when each has the same resolving power.

For SISAM with gratings adjusted for monochromatic light of wavelength λ_j , the intensity expression is identical to that for the conventional Michelson interferometer, Equation 14.

$$I_j(\Delta) = \frac{A_j^2}{2} [1 + \cos (2\pi\Delta/\lambda_j)]. \quad (23)$$

Because the modulation depth quickly approaches zero for other wavelengths, their presence will only add a constant term to the intensity expression. Furthermore, the wavelengths which can reach the detector and cause this offset are limited by the reciprocal linear dispersion of the grating and focusing lens combination and the width of the exit aperture. Thus, for a collection of L narrow lines, the intensity is given approximately by

$$I(\Delta) = 2 S(\lambda) \sum_{j=1}^L \left(\frac{A_j}{2}\right)^2 + \frac{A_0^2}{2} [1 + \cos (2\pi\Delta/\lambda_0)], \quad (24)$$

where $S(\lambda)$ is the slit function of a spectrometer employing the same grating, focusing element, and exit aperture. Thus, if Δ changes linearly with time, the λ_0 wavelength component is modulated according to the cosine term while all other wavelengths are not modulated. Selective amplification of the AC signal leads to the measurement of the intensity of the λ_0 wavelength component. It is not practical to translate one grating to achieve modulation. The usual procedure is to change the optical path difference by rotating the compensating plate.

Spectral scanning is accomplished by tilting the gratings

in unison and changing the values of the Littrow wavelength. The spectrum is measured one component at a time just as in conventional spectrometry and is recorded in the time domain. Thus, no Fourier Transform is required. The requirement of accurate knowledge of path difference is also eliminated since no interferogram results.

The difficulty which is generated stems from the exceedingly high resolving power which is achievable with SISAM. In order to maintain maximum modulation depth for the signals, the grating angles must match to very close tolerances. The tolerance required can be estimated as follows:

From the grating equation for the first order

$$\lambda = 2d \sin \theta.$$

Differentiating,

$$d\lambda = 2d \cos \theta d\theta$$

is obtained. Because $R = \lambda/d\lambda$, $d\theta$ may be obtained as

$$d\theta = (\tan \theta)/R.$$

$d\theta$ represents the grating angle uncertainty corresponding to the wavelength uncertainty $d\lambda$. But the wavelength uncertainty of each grating should be less than one tenth of the resolution to insure adequate matching. Thus, the maximum tolerable uncertainty, U , in each grating angle is

$$U = \frac{d\theta}{10} = \frac{\tan \theta}{10 R}. \quad (25)$$

Evaluating this for typical values of θ ($= 10^\circ$) and R ($= 2 \times 10^4$) gives $U = 9 \times 10^{-7}$ radians or 5×10^{-5} degrees of arc. This corresponds to 0.2 arc seconds. Thus, in SISAM, the require-

ment of accurately knowing the optical path length is traded for the requirement of keeping the grating angles matched.

It is possible to align the gratings at a fixed angle and then change the wavelength by pressure scanning because the grating equation is actually $n\lambda = 2d\mu \sin \theta$ where μ is the refractive index of the medium in which the grating is placed.²⁸ The refractive index of air at atmospheric pressure is 1.0003 and thus is often omitted from the grating equation.⁴² This technique eliminates the mechanical difficulties of turning the gratings synchronously, but the free spectral range is quite small being only a few parts per thousand of the wavelength at one atmosphere. It is also possible to eliminate this tolerance problem for the most part by turning both gratings on the same grating table.³⁸ However, the resulting instrument is far more optically complicated in terms of numbers of surfaces and their alignment.

It may seem curious that SISAM works at all since fringes of equal inclination are formed, but the optical path difference changes along the cross section of the beam. This is most easily explained by considering the interaction of plane waves with a grating. A plane wave front striking a grating is diffracted by each groove. Division of wave front occurs and therefore all of the grooves are coherent sources producing cylindrical waves. Constructive interference only occurs in directions where the crests of the advancing cylindrical waves line up. This combination of cylindrical wave

fronts results in plane wave fronts. The angles at which this occurs correspond to the various diffraction orders of the grating. This can be illustrated geometrically by combining sets of concentric circles such that the centers are equally spaced along a line (Figure 5).

SEMIDS

A cross between the Michelson interferometer and SISAM was first described by Dohi and Suzuki and later investigated by Fitzgerald, Chester, and Winefordner who named it Selectively Modulated Interferometric Dispersive Spectrometer (SEMIDS).^{43,44} SEMIDS (Figure 6) uses a grating as the reflecting element in one arm and a mirror in the other. The main advantages of this are that no Fourier Transform is required (since the instrument behaves basically like SISAM) and that with only one grating to turn, the mechanical tolerance limitations are greatly reduced. The same grating angle tolerance is required in terms of wavelength accuracy, but this is exactly equivalent to the wavelength accuracy of a conventional spectrometer with the same grating and focusing element. Thus, implementation of SEMIDS in the uv-visible spectral region is possible.

Discussions of fringe formation and resolving power parallel those for SISAM and reach the very same results. The intensity expression is a bit different, however, due to an extra contribution of light to the DC level because dispersion does not occur in the mirror arm. The simplified

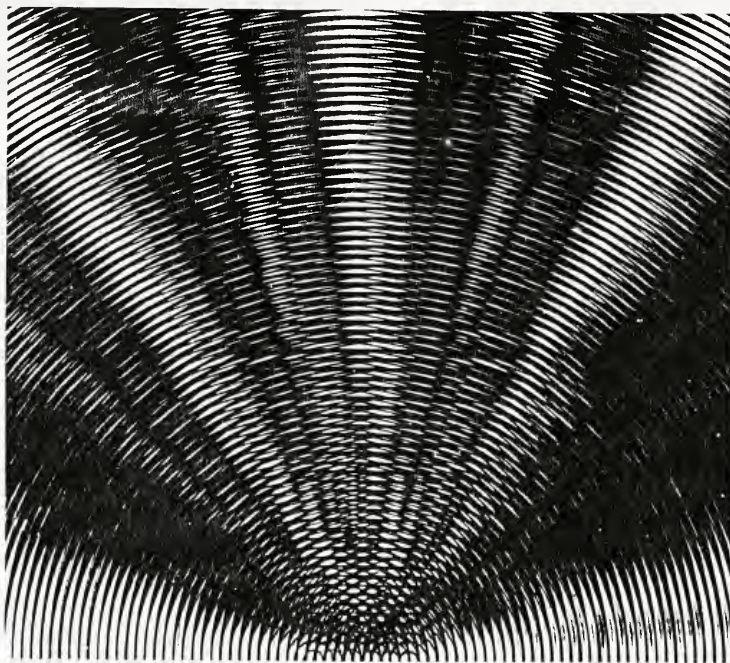


Figure 5. Representation of interference at a grating surface. Six superimposed sets of concentric circles with centers equally spaced along the bottom edge.

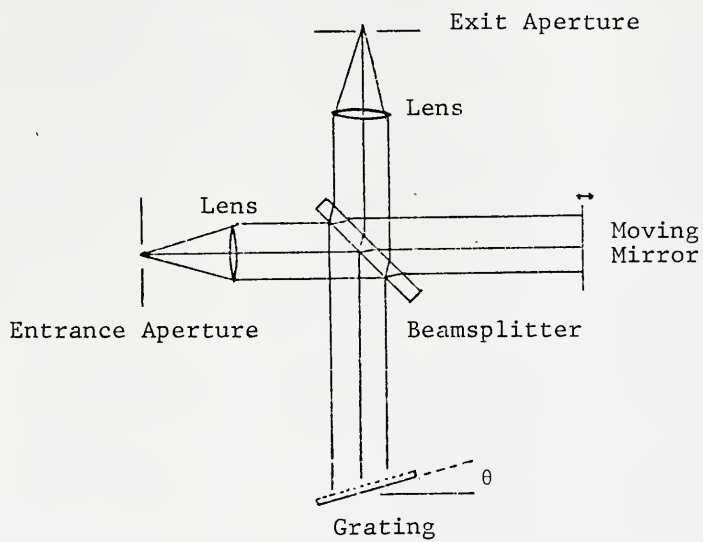


Figure 6. The SEMIDS spectrometer.

intensity expression for a collection of lines can be shown to be

$$I(\Delta) = \sum_{j=1}^L \left(\frac{A_j}{2}\right)^2 + S(\lambda) \sum_{j=1}^L \left(\frac{A_j}{2}\right)^2 + \frac{A_o^2}{2} [1 + \cos (2\pi\Delta/\lambda_o)], \quad (26)$$

where the first summation is the intensity of non-interfering wavelengths contributed from the mirror arm, the second summation is the intensity of non-interfering wavelengths contributed from the grating arm, and the third term is the intensity of the signal wavelength as a function of path difference.

Dohi and Suzuki give an argument leading to the maximum permissible collection solid angle and find it to be $\Omega_M = 4\pi/R$.⁴³ This is twice the value for either the Michelson interferometer or SISAM. The reason for this difference was not discussed.

SEMIDS can be modulated by either turning a compensator plate or by translating the mirror. Both instruments reported thus far have chosen the latter.⁴³⁻⁴⁵ Problems concerning modulation and demodulation arise in practice. These are discussed in Chapter III.

CHAPTER III THE SEMIDS INSTRUMENT

A detailed schematic diagram of the SEMIDS optical system is given in Figure 7. Also, details of each physical and optical component are given in Table I. Electronic components are listed in Table II. Descriptions which have already been published will not be reproduced here.⁴⁴ Rather, emphasis will be placed on important considerations which were previously omitted.

Alignment

An alignment procedure has already appeared in the literature.⁴⁴ However, the procedure does not adequately discuss the detail and significance of proper grating orientation.

If zero order and first order reflections of the same single wavelength are used to align the grating, it is possible that interference fringes of equal inclination can be produced in both orders for this wavelength. This insures that every wavelength will produce the desired fringes in zero order, but it is not sufficient to insure this result in first order where the grating is normally used. The simple alignment procedure which previously appeared does not

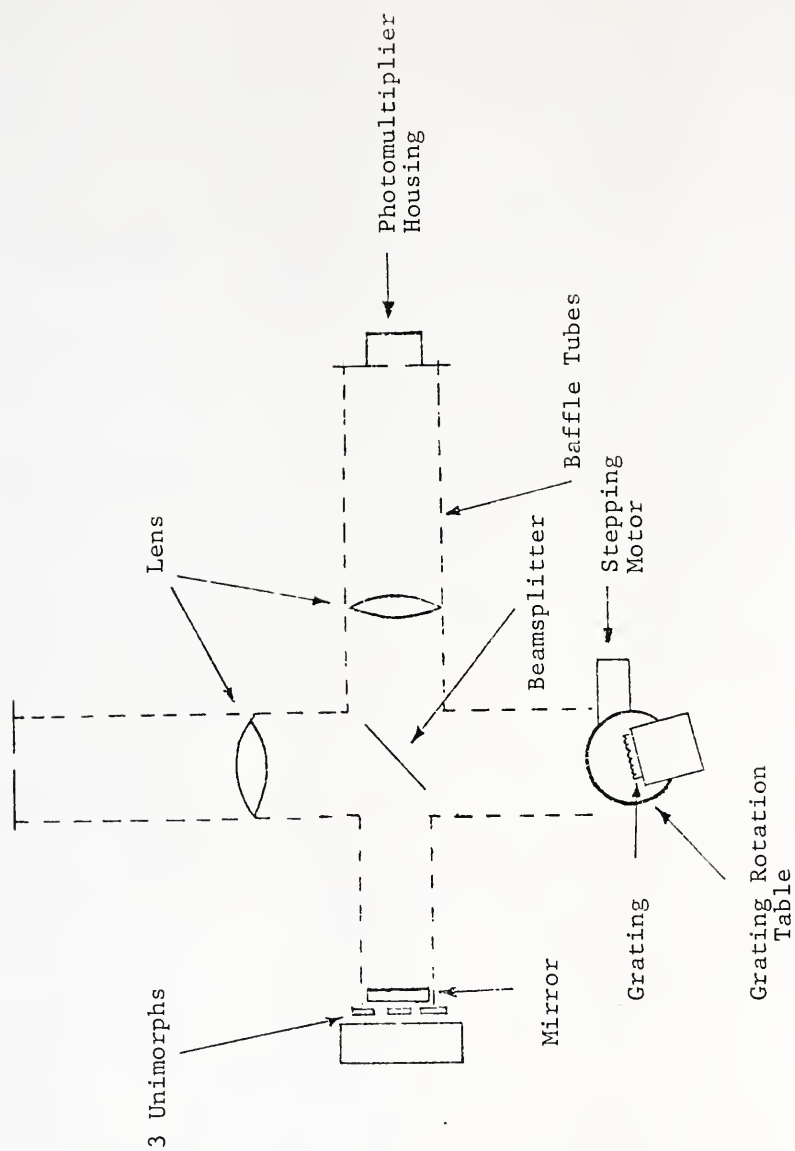


Figure 7. Detailed schematic diagram of optical system.

TABLE I
PHYSICAL AND OPTICAL COMPONENTS

ITEM	MODEL NUMBER OR DESCRIPTION	MANUFACTURER
Lens Mount Beamsplitter Mount Grating Table		Laboratory Con- structed
Grating Orientation Device	10.203	Lansing Research Corp., Ithaca, N. Y.
Mirror Orientation Device	10.503	
Stepping Motor	HDM-15	Responsyn Motor, USM Corp., Goar System Division, Wakefield, Mass.
Collimating and Focusing Lenses	3 inch diameter, 8 inch focal length, biconvex, Suprasil quartz	Esco Products, Oak Ridge, N. J.
Grating	40 mm, 590 grooves/mm, 3.9° blaze angle	Jarrell-Ash Division, Fisher Scientific Co., Waltham, Mass.
Mirror	2 inch diameter, aluminized, $\lambda/10$ flatness	Dell Optics, North Bergen, N. J.
Beamsplitter	3 inch diameter, dielectric coating, $\lambda/20$ flatness	Dell Optics, North Bergen, N. J.
Piezoelectric Transducers	Unimorph	Vernitron Piezo- electric Division, Bedford, Ohio

TABLE II
ELECTRONIC COMPONENTS

ITEM	MODEL NUMBER OR DESCRIPTION	MANUFACTURER
Photomultiplier Tube	1P28	RCA, Harrison, N. J.
Current to Voltage Converter	Laboratory Con- structed from Op- erational Ampli- fier Model 40J	Analog Devices, Inc., Cambridge, Mass.
Photomultiplier Power Supply	280	Princeton Applied Research, Princeton, N. J.
Selective Amplifier	210	
AC Amplifier	211	
Multiplier/Averager	230	
NIM Bin	401 A	Ortec, Inc., Oak Ridge, Tenn.
Square Root Module	Laboratory Con- structed from Multiplier/Divider Model 426 A	Analog Devices, Inc., Cambridge, Mass.
Recorder	XKR	Sargent-Welch
Signal Generator	110	Wavetek, San Diego, Calif.
Signal Generator	180	
Unimorph Driver Amplifier		Laboratory Con- structed
Counter	106 A	Monsanto, West Caldwell, N. J.
High Voltage Power Supply		Heath Co., Benton Harbor, Mich.
Oscilloscope	545 A	Tektronix, Portland, Ore.
Dual Trace Plug-In Unit	Type 1A1	

describe any effort to adjust the grating table rotation axis relative to the optical plane.⁴⁴ If this adjustment is not made or is incorrectly made, it is still possible, using a single wavelength, to produce fringes of equal inclination in zero and first orders. The zero order fringe can be centered by tilting the grating using the tilt micrometer on the grating orientation device, while the first order fringe can be centered by turning the grating about an axis normal to its surface. Unless the grating table rotation axis is perpendicular to the optical plane (defined by the intersection of the axes of the two reflecting arms), the reflected ray from the grating will only intersect the optical plane at the two grating angles, i.e., $\theta = 0$ (zero order) and $\theta = \arcsin(\lambda/2d)$, where λ is wavelength for which the first order adjustment was made. All other reflections will be out of the plane.

The first step in the proper alignment procedure is to make the grating table rotation axis perpendicular to the optical axis of that arm of the interferometer. This is analogous to the alignment requirement for a grating in a scanning dye laser. Thus, the same basic procedure may be employed for this part of the grating alignment in SEMIDS. A dye laser manual may be consulted with suitable adaptations made for hardware differences.⁴⁶ This alignment can be done with only the entrance aperture and the grating installed on the base plate and must be done without the collimating lens. The main point of this procedure is that the grating

rotation axis becomes the reference by which all other adjustments are made including those of the He-Ne alignment laser. It is absolutely incorrect to adjust the laser to strike the exact center of the grating without further assurance that this ray is perpendicular to the grating table rotation axis.

Once this step is completed, the mirror and beamsplitter can be installed. The beamsplitter must be erect so that the ray transmitted to the grating is not displaced vertically. Some horizontal displacement will occur due to the thickness, refractive index and angle of the beamsplitter, but this is of no consequence. The grating reflection is then aimed directly at the mirror as shown in Figure 8. The plane defined by the ray striking the grating and by any of its reflections (which are now coplanar for all values of θ) must also contain the axis of the mirror arm. Thus, the ray directed to the mirror from the beamsplitter must intersect the ray now aimed at the mirror from the grating. If an adjustment is necessary, the beamsplitter must be the element to be tilted. Further refinements in the beamsplitter adjustment can be made by rotating the mirror so that its reflection is aimed at the grating and the mirror and grating reflections aimed at each other share the same path. Thus, a Sagnac interferometer is produced.⁴⁷ Adjustments to either the beamsplitter, the mirror, or the grating angle may be made while observing the interference produced in the exit arm. Production of fringes of equal inclination for at least

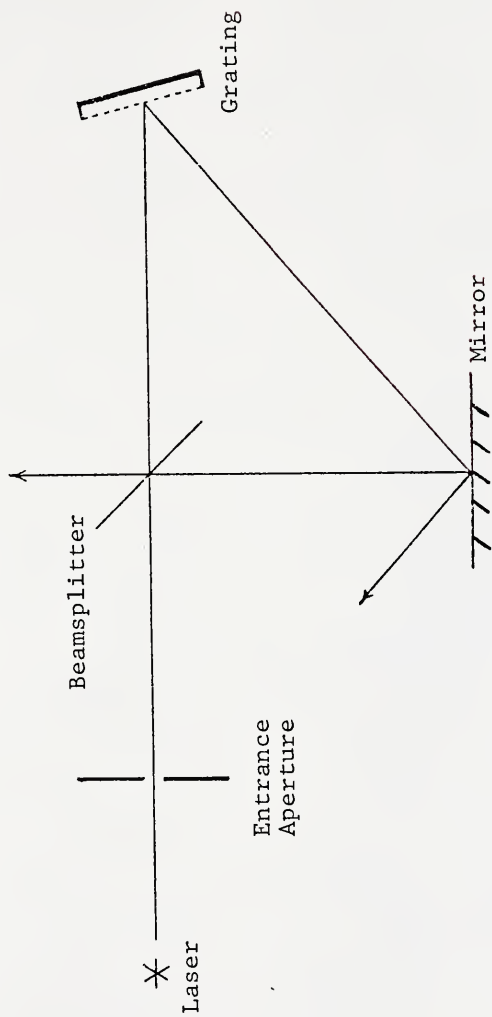


Figure 8. The grating reflection is aimed at the mirror during the beamsplitter adjustment.

three different grating orders insures that all optical paths are in the same plane. (This was never done with SEMIDS due to the limited rotation of the mirror orientation device. As a result, the alignment was never fully optimized.) The remainder of the alignment is completed in the manner already described.⁴⁴ Extreme care must be exercised in making the height and tilt adjustments for the collimator because any error here deflects the optical axis away from the entrance aperture (or, vice versa, deflects the axis out of the previously defined optical plane). If a white card with a clean pinhole is placed over the face of the alignment laser such that the beam shines through the center of the hole and, if the aperture is opened wide, it is possible to observe both of the first reflections from the front and back surfaces of the lens plus a set of concentric circular fringes caused by interference of these two reflections. The lens is properly positioned when all three of these are concentric with the pinhole.

Modulation

Signal modulation in SEMIDS is accomplished by translating the mirror over short distances along its axis. The mirror is mounted on a set of three unimorph piezoelectric transducers.

The unimorph is a wafer of PZT5B ceramic of 1 in diameter which is glued to the center of a brass disc of 1.35 in diameter. The brass side of each unimorph is mounted cir-

cumferentially to a brass ring. Three unimorphs are arranged in an equilateral triangle on the mirror orientation device with the mirror glued directly to the ceramic discs. A bias voltage is applied to each unimorph to flex it away from the mount, i.e., to make the ceramic side convex. The programmed displacement voltage is then superimposed on the bias voltage. To flex the unimorph in this manner, it is necessary that the bias voltage oppose the poling direction of the ceramic. Sustained operation in this manner may cause the ceramic to repole in this opposite direction. This actually occurred on one occasion resulting in one transducer attempting to displace in the direction opposite that of the remaining two. The problem was solved by purposely repoling the ceramic in the original direction by momentarily applying a DC voltage of -800 V to the ceramic while the brass was grounded.

Inspection of Equation 26 reveals that the intensity will be modulated as a cosine function if Δ changes linearly with time, i.e., if the path difference is changed at a constant velocity. The path difference changes at twice the velocity of the mirror. Thus, if $\Delta \propto 2vt$ where v is the mirror velocity and t is time, the argument of the cosine term becomes $4\pi vt/\lambda_0$. Therefore, the modulation frequency is $f = 2v/\lambda_0$.

The mechanical problems of maintaining mirror adjustment and velocity accuracy over long excursions of the mirror are acute in the uv-visible spectral region. The tolerances re-

quired can be greatly reduced by repetitively analyzing the same one or two fringes. Figure 9a shows that a triangular mirror displacement of $\lambda/4$ can produce the same interference modulated signal as the application of a constant mirror velocity. However, the phase of the applied triangular displacement must match the fringes so that the direction of the mirror is reversed at the interference maxima and minima. Figures 9b and 10a and b show the resultant signals for a variety of other phase conditions. Notice that for a phase offset equal to $\lambda/8$, the modulation frequency is doubled, and the signal amplitude is divided by 2.

It is not possible to fix and maintain any phase relationship between Δ and the interference for two reasons. First, the path difference is not constant but varies across the width of either arm due to the grating angle, θ . (However, for the Littrow wavelength in the first order, the path difference between rays parallel to the axis and striking adjacent grooves of the grating is λ . The path difference between any two such rays is $\eta\lambda$ where η is the number of grating grooves separating the rays.) The intersection of the grating surface and the axis may be used to calculate Δ for evaluating the intensity expression. If the rotation axis of the grating table does not also intersect this point, then Δ will change with the grating angle θ as is illustrated in Figure 11. This is an exceedingly difficult, if not impossible, adjustment in the uv-visible spectral region and was not even attempted. Second, there is no benefit in compensating the beamsplitter in SEMIDS so that Δ is "fixed"

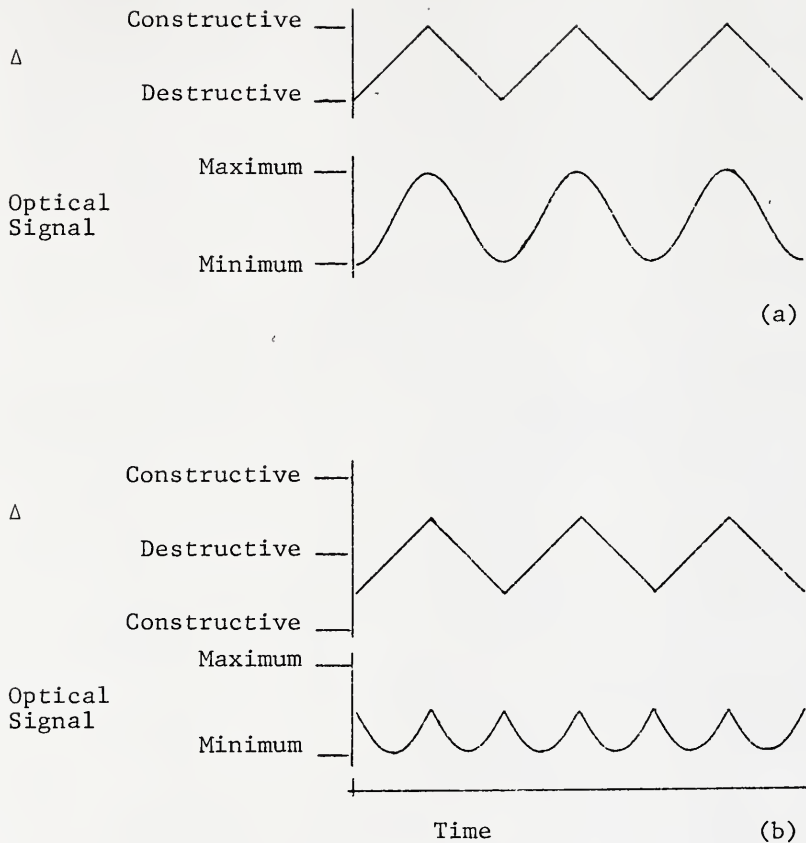


Figure 9. (a) The optical signal resulting from a triangularly varying path difference is identical to the signal obtained from a linearly varying path difference for the phase condition shown. (b) The signal after a phase shift corresponding to $\lambda/8$ has occurred.

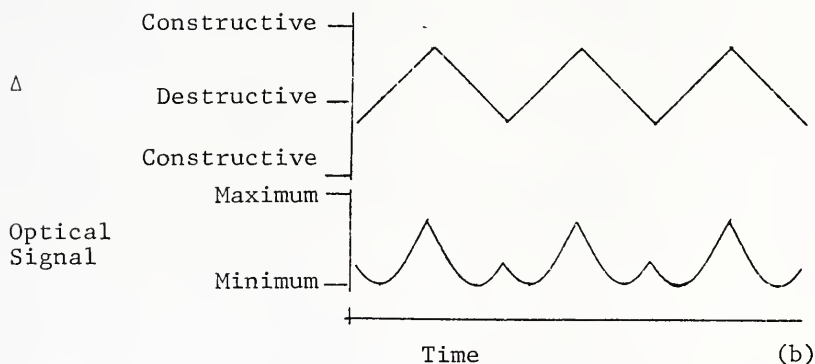
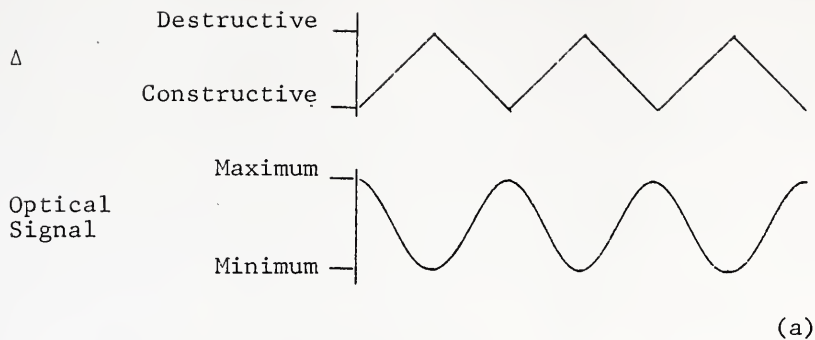


Figure 10. Signals for other phase conditions.
 (a) Phase shift corresponding to $\lambda/4$ compared to Figure 9 (a). (b) Phase shift corresponding to $\lambda/16$ compared to Figure 9 (a).

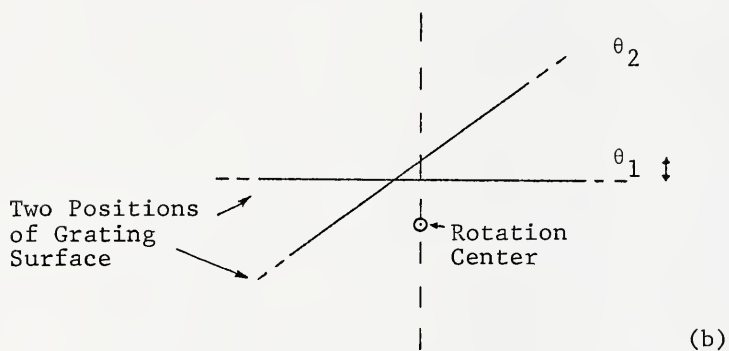
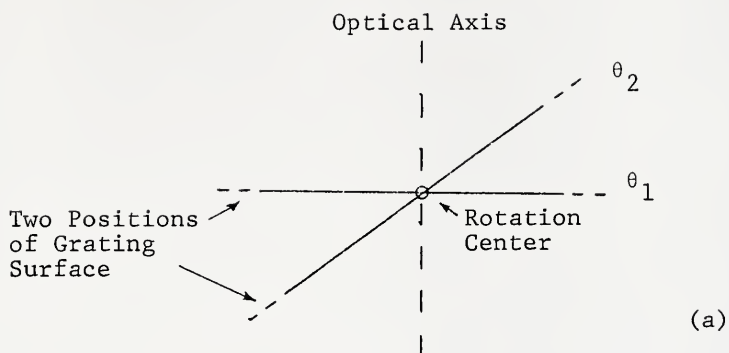


Figure 11. (a) Proper grating surface position on the rotation axis. (b) Improper position results in a path length change when the grating is turned, as shown by the double arrow.

vs. λ as in the Michelson interferometer (except for the useless triumph experienced by viewing a white light fringe for $\Delta = 0$ in zero order); this has been discussed above. Thus, Δ also varies in SEMIDS due to the optical asymmetry of the beamsplitter.

A zero phase error relationship, i.e., one always resulting in the signal shown in Figure 9a, can be established by generating a phase error signal from the signal itself.^{40,48} This error signal can be applied as negative feedback to the bias voltage of the transducer assembly. Thus, phase-locked conditions will be maintained as long as a sufficiently pure signal exists, and therefore this technique will work well for absorption spectra with a SISAM spectrometer because the instrument is essentially analyzing a bright source. This solution fails, however, when faint emission signals are to be measured and, especially for SEMIDS, when background radiation at other wavelengths is present which seriously degrades the observed signal-to-noise ratio. (See Chapter IV regarding signals and noises.)

The alternate approach to establishing a fixed phase condition is to modulate the phase error by modulating the transducer bias voltage.⁴³ Since this double modulation approach requires the simultaneous application of two frequencies to the mirror assembly, the frequency response of the unimorph/mirror combination was measured. The results are plotted in Figures 12 and 13 for both triangular and sinusoidal driving signals. In both cases, the relative

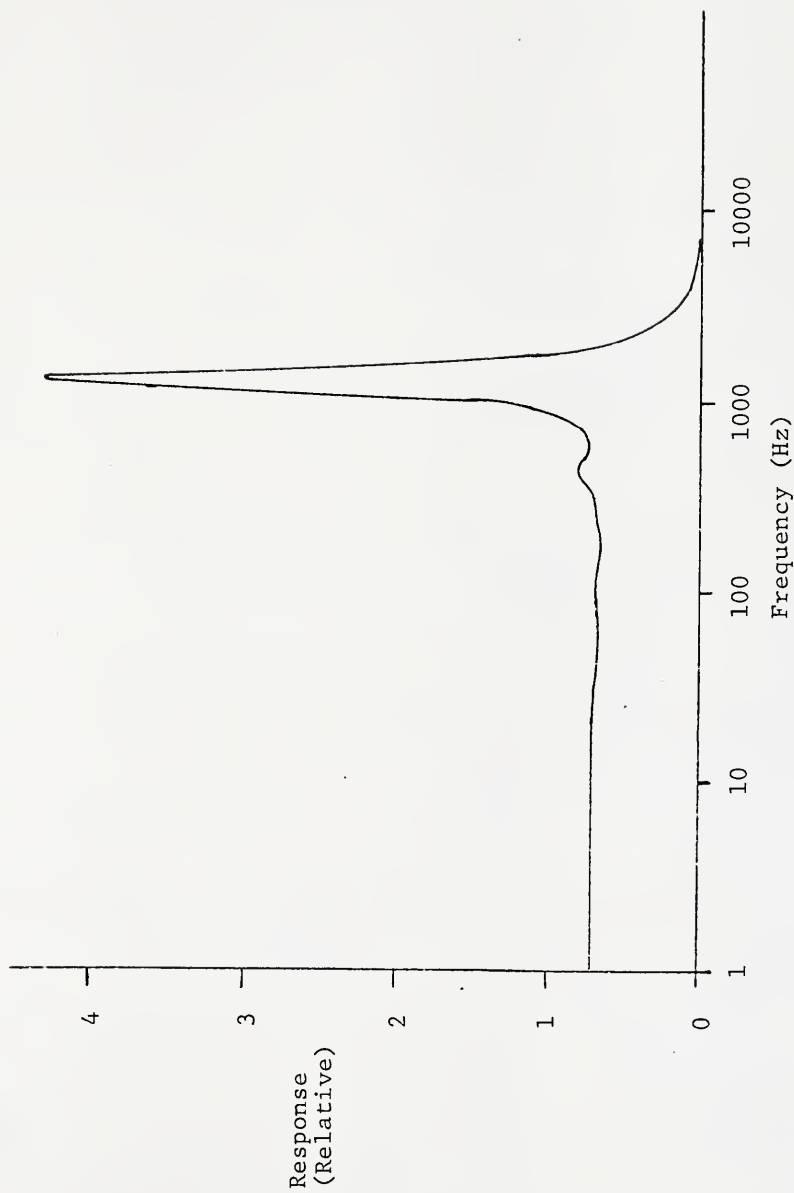


Figure 12. Unimorph-mirror frequency response for triangular driving signals.

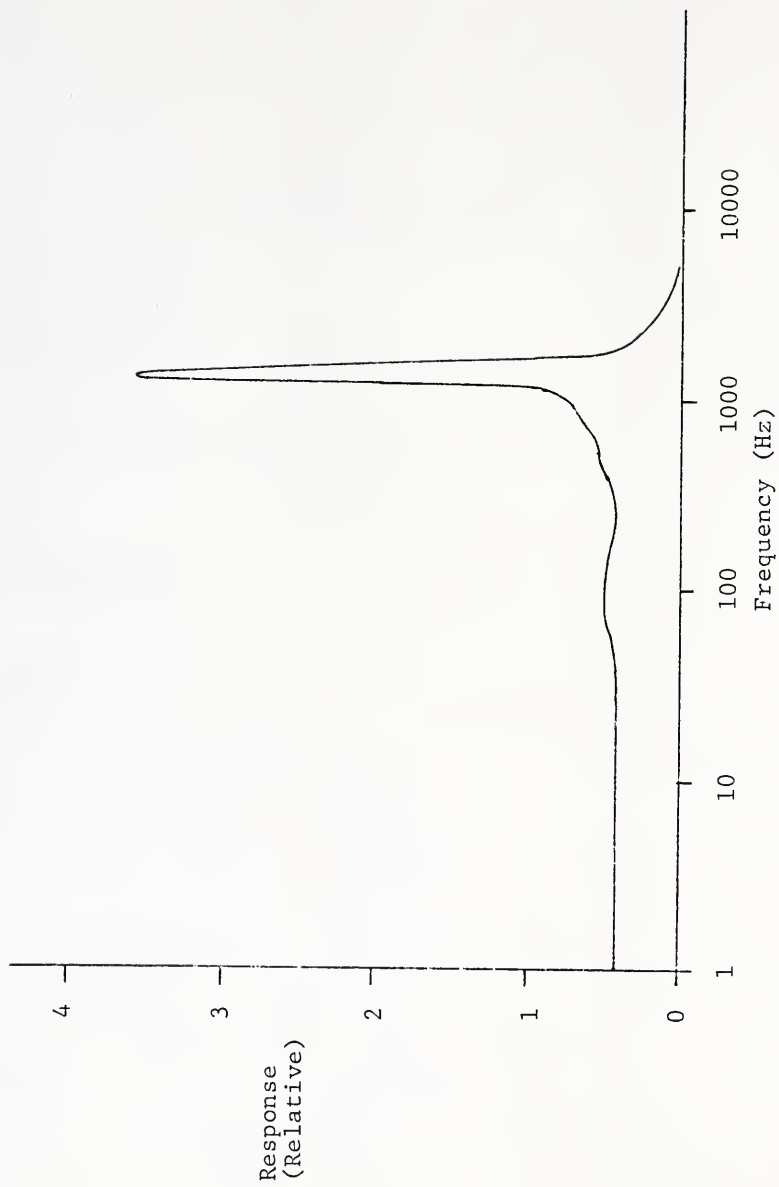


Figure 13. Unimorph-mirror frequency response for sinusoidal driving signals.

response has units of distance per volt and was calculated from the peak-to-peak voltage required to displace the mirror $\lambda/4$, where λ was the 632.8 nm He-Ne laser line. Distance was measured by observing the resultant intensity of the interference with the photomultiplier tube. The photocurrent was converted to voltage and monitored with the oscilloscope. The bias voltage was set to produce zero phase error and was periodically readjusted as required. Accurate triangular displacement of the mirror will produce a perfect sinusoidal variation in the intensity. However, severe harmonic distortion was observed in the photo-signal when the applied triangular wave was in the region of ca. 150 to 650 Hz. The low frequency triangular waves contain even harmonic frequencies descending in amplitude with increasing frequency. However, if one of these harmonic frequencies falls near the resonance frequency of the mirror system, oscillation of the mirror becomes too large with respect to the amplitude component needed at this frequency to approximate the triangular function.

The distortion (described above) vanished when a sinusoidal drive was used. However, other harmonic distortion is introduced since the drive is not at constant velocity. Consider the intensity expression for SEMIDS adjusted to a monochromatic source:

$$I(\Delta) = \frac{A^2}{2} [1 + \cos (2\pi\Delta/\lambda)]. \quad (27)$$

Instead of considering Δ varying linearly with time, let

$$\Delta(t) = \Delta_0 + \frac{\lambda}{4} \cos(2\pi ft),$$

where $\lambda/4$ is the peak path difference contributed by the cosine function, f is the frequency of the sinusoid, t is time, and Δ_0 is the path difference for the bias voltage alone. Substituting into Equation 27

$$I(t) = \frac{A^2}{2} \{1 + \cos[2\pi\Delta_0/\lambda + \frac{\pi}{2} \cos(2\pi ft)]\} \quad (28)$$

results. The harmonic content of this expression can be found by performing a cosine Fourier Transform. However, this yields an integral which is not easily solved. A plot of $I(t)$ over one period is shown in Figure 14 for $\Delta_0 = \lambda/4$ (which is required for no phase error). A guess at the harmonic content can be made by observing the squared appearance of the wave, which indicates frequency components at the odd harmonics. Because most of the signal power is still at the fundamental frequency and because the waveform is accurately reproduced for all applied frequencies, a sine wave drive was considered a reasonable alternative to triangular wave drive.

A number of other considerations are required in choosing the proper frequencies, waveforms and amplitudes for the two signal components applied to the mirror drive.

For $\lambda/4$ peak to peak mirror excursion at a single frequency, f , the resultant photo-current is composed of (at least) two frequency components, f and $2f$, depending on the initial path difference as illustrated in Figures 9 and 10.

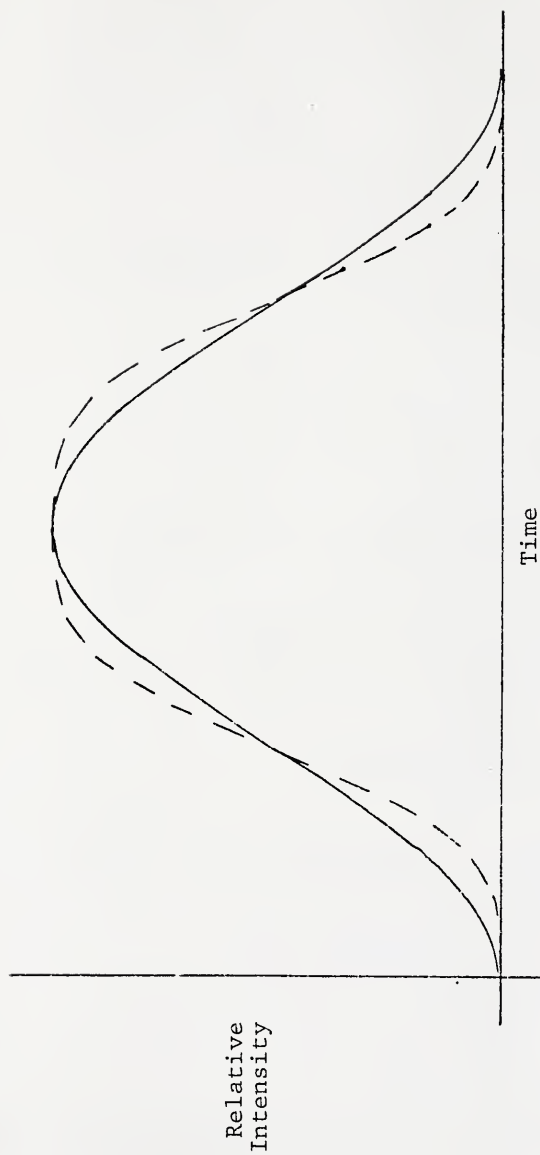


Figure 14. One period of SEMIDS optical signal for (in-phase) sine wave drive (dashed line) shown with a pure sine wave (solid line).

Suppose that the initial path difference is adjusted to give in-phase modulation (Figure 9a). A drift of $\lambda/8$ in the initial path difference caused by thermal expansion of the base plate or by changing the grating angle will result in the modulated signal being shifted to $2f$. If an electronic band pass filter is used to reduce white noise and is set to frequency f , its output would now be zero. Thus, a 100 % error can occur depending on the phase between path difference extremes and interference maxima and minima if single frequency modulation is used. Now, if the bias voltage is also modulated at a lower frequency with a $\lambda/4$ peak to peak excursion, the phase difference is made to oscillate. A large fraction of the signal occurs at frequency $2f$ and thus is not measured, but the fraction of the total signal remaining at f should be nearly constant, regardless of the phase.

In actual fact, things are not this simple. Consider Equation 28 but now with Δ_0 modulated by a low frequency sinusoid, i.e., let

$$\Delta_0 = \Delta_B + X_L \cos (2\pi f_L t).$$

Equation 28 becomes

$$I(t) =$$

$$\frac{A^2}{2} \{1 + \cos [\frac{2\pi}{\lambda} (\Delta_B + X_L \cos (2\pi f_L t)) + \frac{2\pi}{\lambda} X_U \cos (2\pi f_U t)]\}$$

(29)

where f_L is the lower applied frequency, f_U is the upper, X_L and X_U are the peak mirror displacements for the lower and

upper frequencies, respectively, and Δ_B is the path difference for the unmodulated bias voltage only. Plots of $I(t)$ vs. t for two values of Δ_B and for X_L and $X_U = \lambda/4$ are given in Figures 15 and 16. Oscilloscope traces of the actual observed signals are given along with the mirror drive signal in Figure 17.

When filtered about the frequency f_U , the intensity signals resemble the result of double sideband modulation of the frequency f_L by the frequency f_U .⁴⁹ Thus, there is little or no signal power at the frequency f_U . It resides in the sidebands positioned at $f_U \pm f_L$.

Figure 5 in reference 43 shows another condition in which the phase is intermediate to the cases above. The filtered signal now has beats of alternating size. The nodes are periodic at a frequency of approximately $3 f_L$. Thus, the bandpass filter must pass the sidebands at $f_U \pm 3 f_L$ without much attenuation to just approximately preserve the signal.

The total signal power in the vicinity of f_U remains constant. However, the actual power distribution among the sideband frequencies shifts with the phase between the mirror movement and the interference maxima and minima. Thus, in order to reject as much noise as possible with the bandpass filter while passing nearly all of the signal information, f_L must be as low as possible so that the sidebands occur very near f_U and a small bandpass may be used. However, because the beats occur at a frequency of no lower than $2 f_L$,

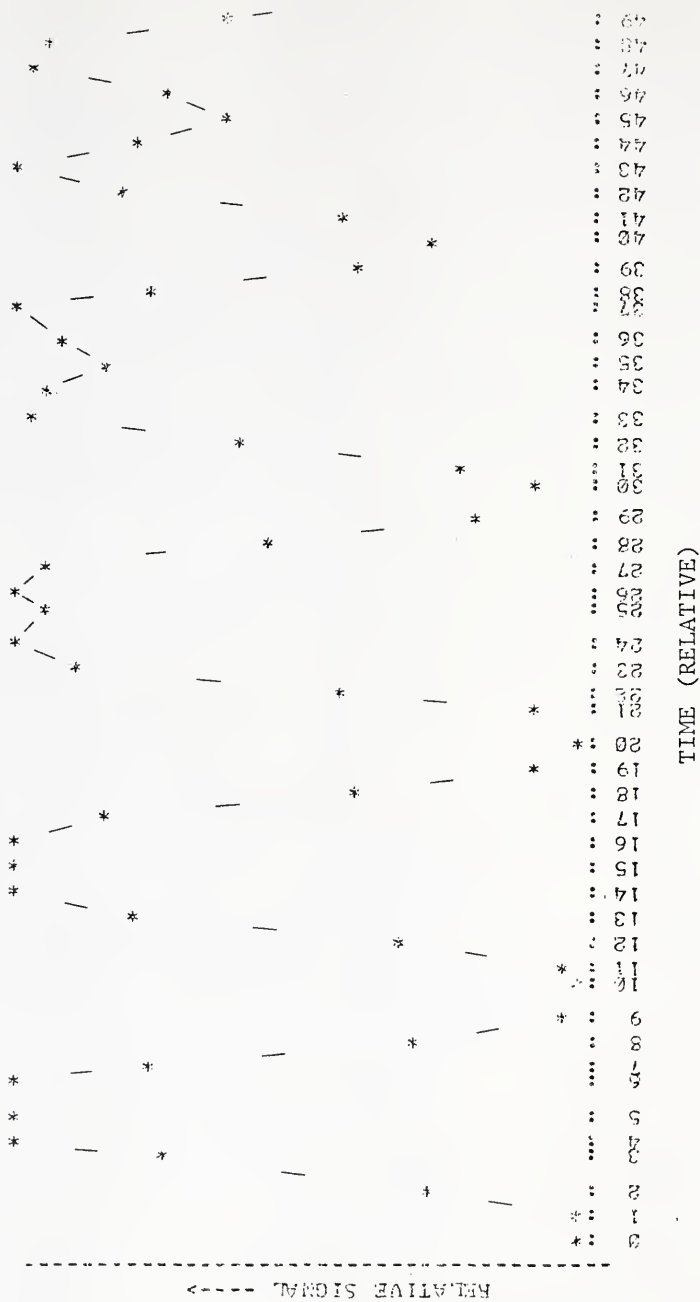


Figure 15. Plot of intensity function (Equation 29) vs. time for one period.
 $X_L = X_U = \lambda/4$. $\Delta_B = 0$. (a) First quarter of period.

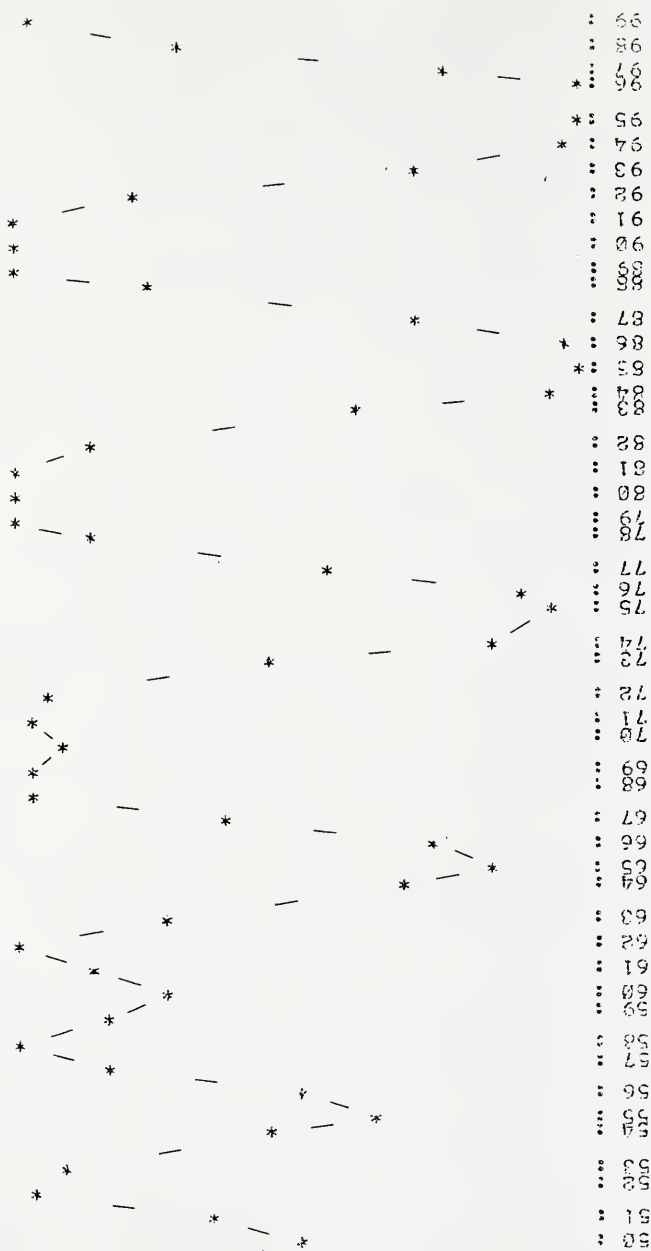


Figure 15. (b) Continuation of time base from previous page. Second quarter of period.

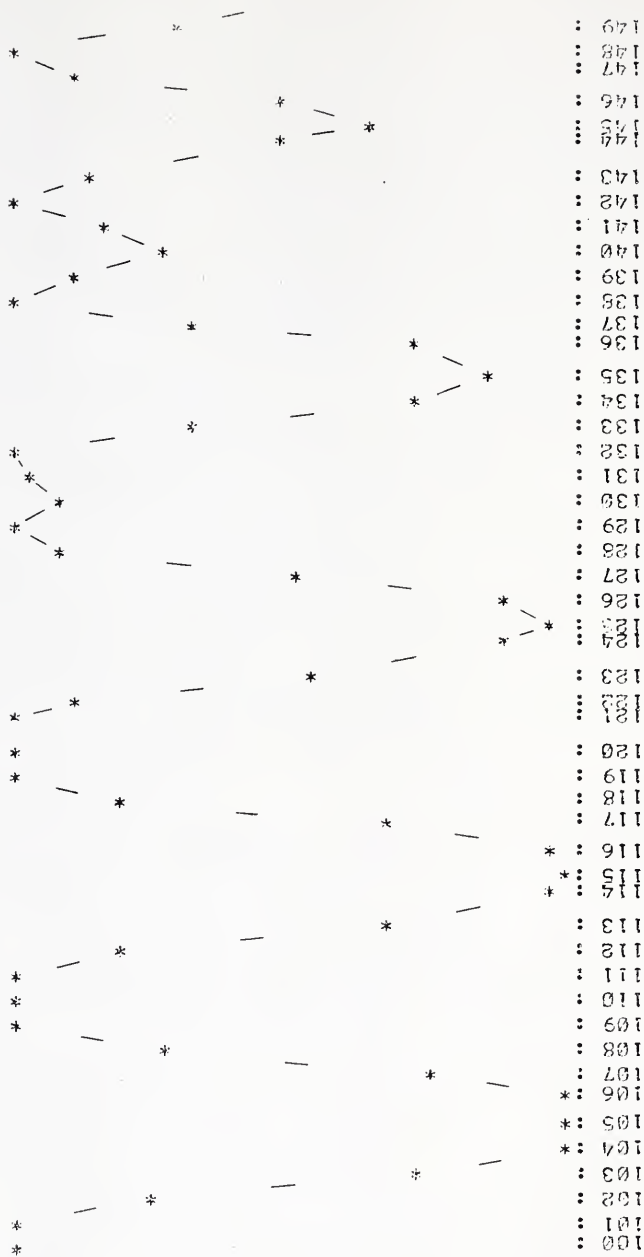


Figure 15. (c) Continuation of time base from previous page. Third quarter of period.

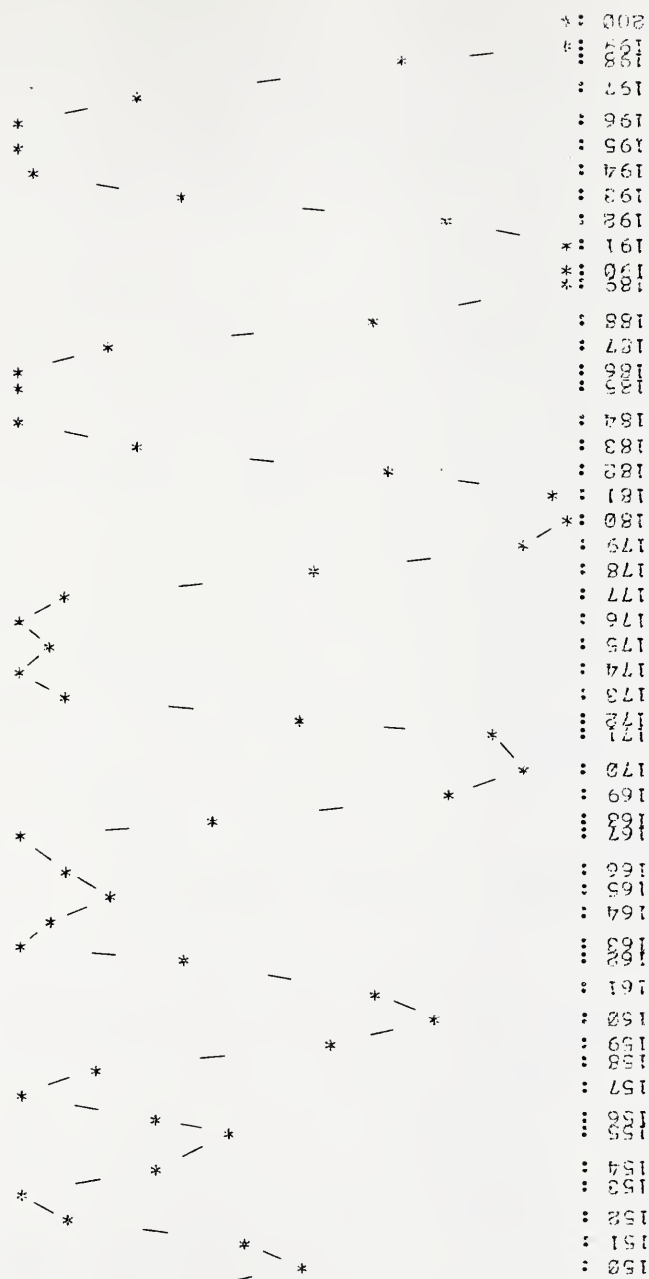


Figure 15. (d) Continuation of time base from previous page. Fourth quarter of period.

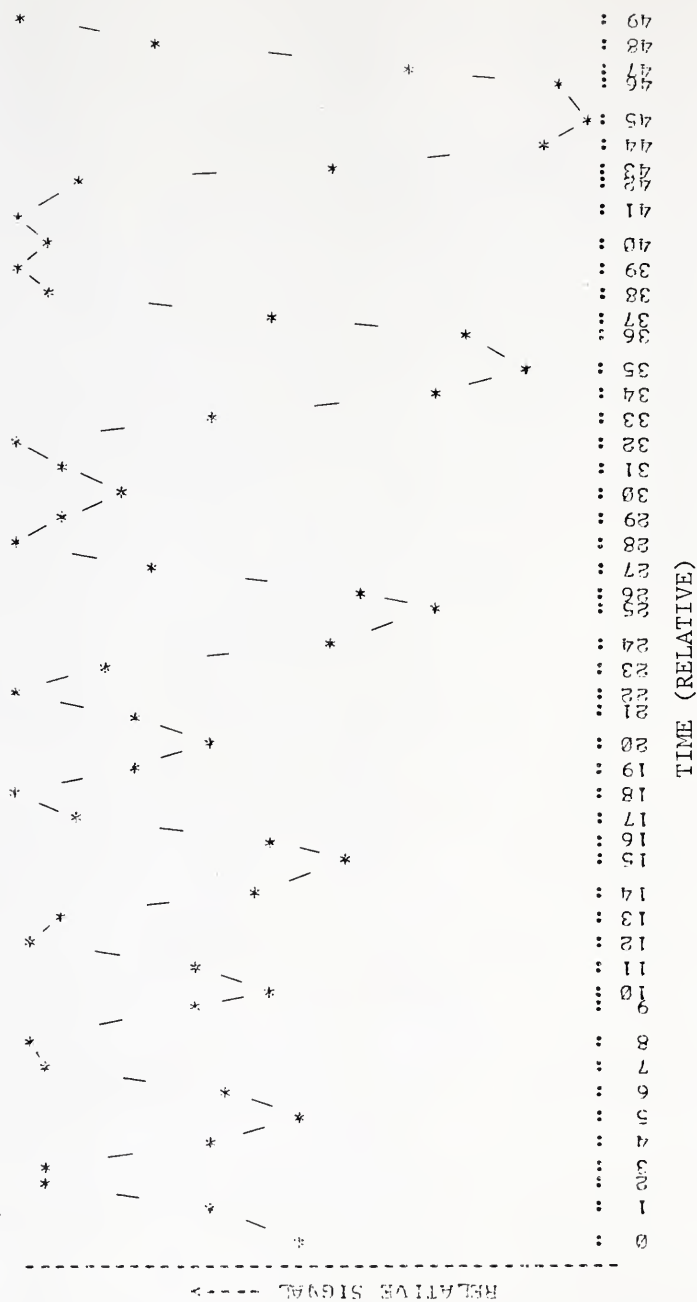


Figure 16. Plot of intensity function (Equation 29) vs. time for one period.

$X_L = X_U = \lambda/4$. $\Delta_B = 3\lambda/4$. (a) First quarter of period.

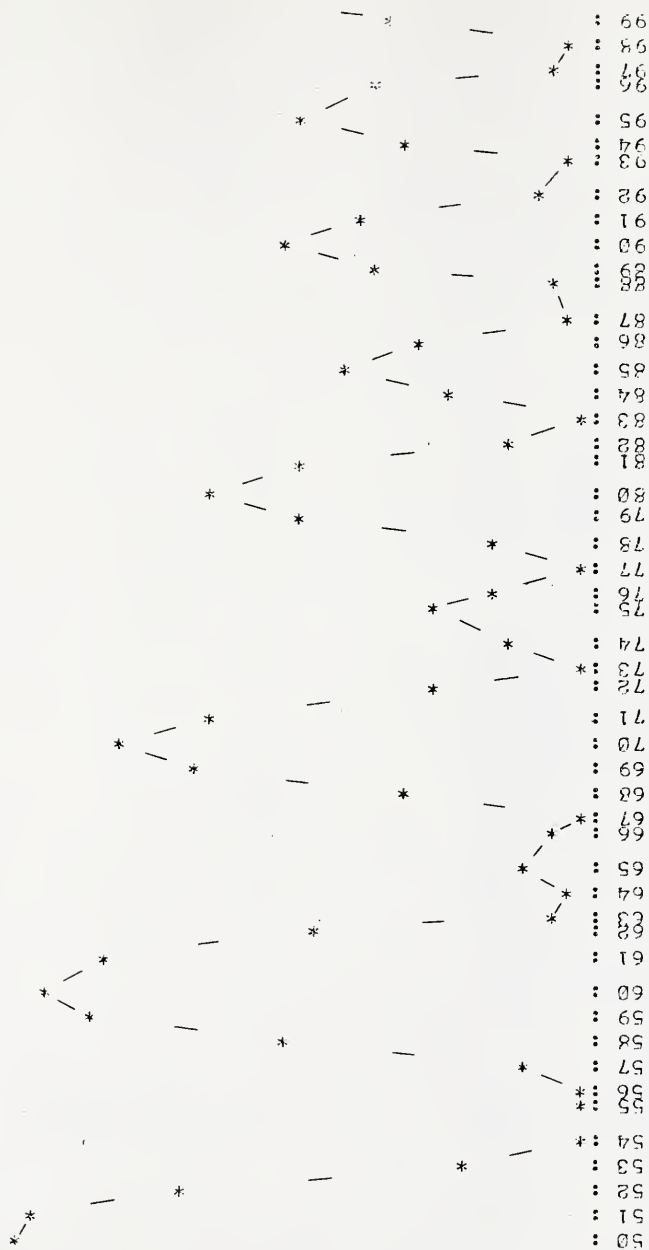


Figure 16. (b) Continuation of time base from previous page. Second quarter of period.

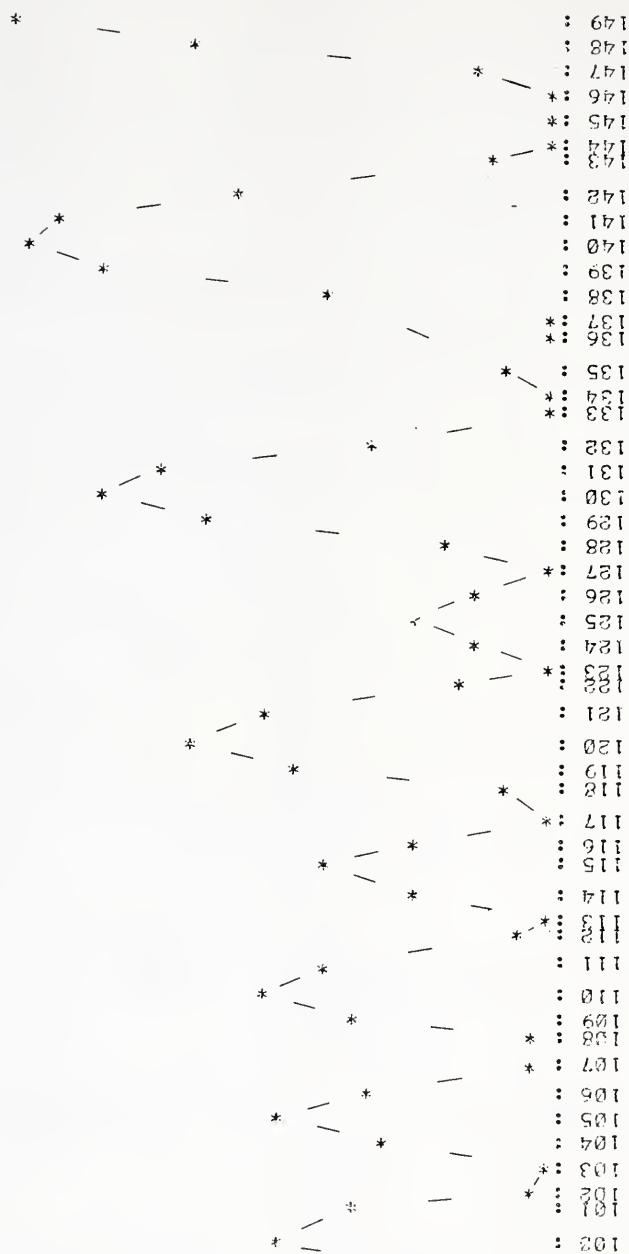


Figure 16. (c) Continuation of time base from previous page. Third quarter of period.

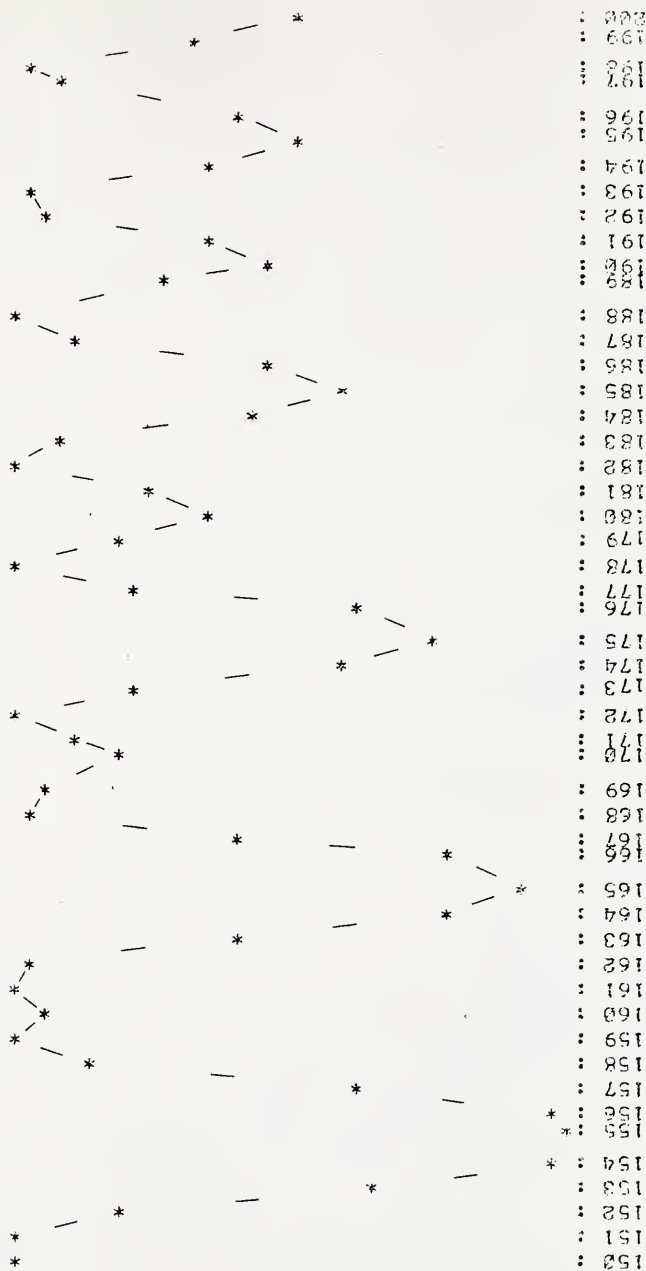
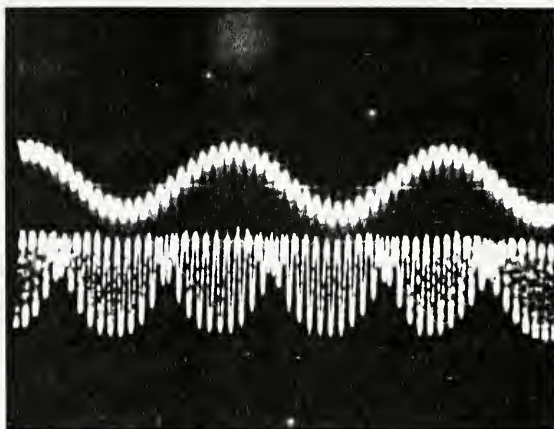
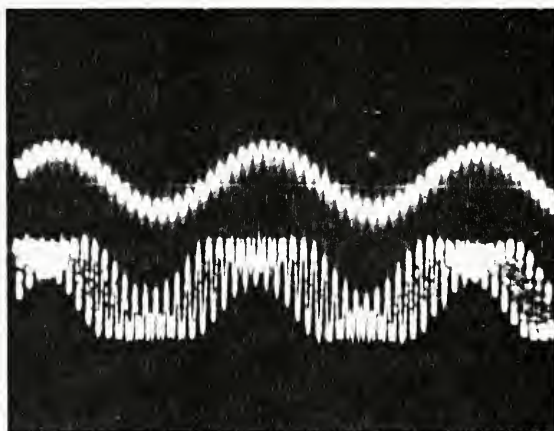


Figure 16. (d) Continuation of time base from previous page. Fourth quarter of period.



(a)



(b)

Figure 17. (a) Oscilloscope traces of mirror drive signal (upper trace) and observed photo-signal (lower trace) for the conditions given in Figure 15. (b) Similar traces for the conditions given in Figure 16.

this and the time constant chosen limit the minimum value of f_L if ripple on the rectified signal is not to become a new noise source. The condition, in general, for no greater than 1 % ripple on a signal rectified from a frequency, f , is $\tau \geq 10/f$ where τ is the time constant.⁵⁰ Thus, for SEMIDS, $f_L > 5/\tau$ for less than 1 % ripple.

The choice of f_U is not so critical. It was noted experimentally that errors upon phase changes were larger for $f_U < 40 f_L$ than for higher choices of f_U .

X_L and X_U are not restricted to $\lambda/4$ but in general may be any integral multiple of this increment. The main effect in increasing the displacements is that the signal frequencies are also increased. For example, doubling the displacements doubles the observed signal frequencies.

At this point, the relationship between parameters has become so complicated that the final choice between waveforms, amplitudes and filter bandwidth was more easily obtained by experiment. The choice of frequencies and time constant was made based on the previously mentioned considerations. The compromise conditions chosen were $f_L = 25$ Hz, $f_U = 1000$ Hz and $\tau = 300$ ms. The experimental results are given in Table III. Relative average signals were normalized to the highest one observed which was assigned the arbitrary value of 100. The % drift is defined here as the difference between the maximum and minimum signal observed for a given set of parameters divided by their average and expressed as percent. A diffused He-Ne laser beam was used as the source.

TABLE III
EXPERIMENTAL DETERMINATION OF OPTIMUM PARAMETERS

f_L		f_U		Q															
				1		2		5		10		20		50		100			
				$wf\ X_L$	f_d	S	D	S	D	S	D	S	D	S	D	S	D	S	D
1	T	$\lambda/4$	$\$$	$\lambda/4$	f_U	98	8.6	90	8	100	4.2	90	8.2	79	14	59	65	47	111
2	$\$$	$\lambda/4$	$\$$	$\lambda/4$	f_U	90	28	89	26	80	32	73	32	60	32	38	28	33	60
3	T	$\lambda/4$	T	$\lambda/4$	f_U	82	12	82	13	81	8	78	11	64	16	46	67	42	104
4	$\$$	$\lambda/4$	T	$\lambda/4$	f_U	86	32	84	31	77	40	72	35	59	26	40	23	33	64
5	$\$$	$\lambda/4$	$\$$	$\lambda/4$	$2f_U$	72	7	54	12	45	26	35	33	35	33	28	59	24	102
6	T	$\lambda/4$	$\$$	$\lambda/4$	$2f_U$	72	6	54	6	44	10	40	9	34	14	26	37	21	70
7	$\$$	$\lambda/4$	T	$\lambda/4$	$2f_U$	58	14	40	5	30	26	25	33	23	33	17	77	15	114
8	T	$\lambda/4$	T	$\lambda/4$	$2f_U$	60	5	44	4	33	10	30	9	26	14	20	40	18	63
9	T	$\lambda/4$	T	$\lambda/2$	$2f_U$	88	5	79	5	73	6	69	7	61	7	47	18	37	65
10	$\$$	$\lambda/4$	T	$\lambda/2$	$2f_U$	86	8	76	12	71	16	65	18	59	21	46	44	42	50
11	$\$$	$\lambda/4$	$\$$	$\lambda/2$	$2f_U$	84	9	74	13	72	21	67	24	60	18	48	52	40	96
12	T	$\lambda/4$	$\$$	$\lambda/2$	$2f_U$	91	4	81	5	76	6	73	7	63	6	48	20	40	65
13	T	$\lambda/2$	T	$\lambda/2$	$2f_U$	92	5	80	5	72	4	67	7	55	10	39	11	31	44
14	T	$\lambda/2$	$\$$	$\lambda/2$	$2f_U$	89	3	82	4	72	6	67	9	55	15	40	8	30	41

f_L = lower frequency, f_U = upper frequency, $Q = Q$ setting of the selective amplifier,
wf = waveform, X_L = lower frequency mirror displacement, X_U = upper frequency mirror displacement, f_d = frequency detected, T = triangular wave, $\$$ = sine wave, S = signal (relative units), D = % drift (relative to signal).

Phase changes were purposely induced by warping the baseplate with pressure applied from the experimenter's finger to the baseplate edge at an optical axis. Care was taken not to move the instrument significantly and only a slight force (~ 8 oz) was required to change Δ_R by λ , which was the largest distance change made.

General observations of the results show that the sine wave drive for the low frequency component is less satisfactory than the triangular wave drive. The harmonic distortion problem for triangular wave drive does not exist at low frequencies and the use of triangular wave drive for f_L results in the width of the beats formed varying linearly with the phase error. Thus, as one set of beats decreases in width as Δ_R is changed, another set of beats increases its width at the same rate. For f_L as a sine wave and all other parameters set as in cases 13 and 14 in Table III, the drift observed was again much worse. The results were not tabulated.

Because SEMIDS was to be evaluated for flame atomic emission, one more noise source must be considered before a final choice of parameters can be made. This noise is impulse noise which is caused by the occurrence of large droplets or particles in the flame and usually results in a spike being produced at the recorder. The average frequency of occurrence of these impulses limits the maximum time constant which may be employed. For example, if the average frequency of impulses is greater than $1/5\tau$, the electronics would only be recovering from one impulse when the next one occurs.

Thus, the continuous perturbation of the electronics by the impulses can completely obscure the analytical information.

SEMIDS' response to impulse noise was very unusual. The behavior is summarized in Table IV. This behavior is probably due to the ability of the selective amplifier to recover from impulses more quickly at low values of Q . (Q is defined as the ratio of the center frequency to the band-pass of the filter.)

Table IV also summarizes a subject which does not involve any new noise but which may pose a problem under certain conditions. Because no fixed phase relationship between interference and path differences can be maintained, SEMIDS must utilize asynchronous rectification of the modulated signal. Any AC component which is rectified will contribute to the final DC output. Thus, flame and other background noise which is within the bandpass of the selective amplifier will generate a DC level at the output, even with no analyte present. The noise on this DC level is determined by the time constant chosen. Thus, the offset will depend to a large extent on the Q chosen but the noise will not. Typical behavior is shown in Table IV. In cases where fixed phase relationships exist between a modulator and the resultant signal, synchronous or "lock-in" rectification may be employed. Since the phase of the noise components is random, the average value of the rectified noises is zero, and the offset problem is eliminated.

Case 14 from Table III has the best signal and drift

TABLE IV
NOISE BEHAVIOR VS. Q

Q	Shot Noise Offset V DC	Peak to Peak Baseline Noise V DC	Average Peak Impulse Voltage V DC
1	3.90	0.25	<-1.5
2	2.65	0.25	-1.5
5	1.50	0.25	+0.4
10	0.95	0.25	+0.9
20	0.55	0.22	+1.5
50	0.25	0.18	+2.6
100	0.15	0.14	+3.3

Measurement conditions:

10 ppm Na solution aspirated into flame (see Table IX)

Apertures set at 5 mm

650 V DC applied to PM tube

Transconductance factor = 10^7 V/A

Selective amplifier set at 2 kHz with gain = 10

AC gain = 20

AC coupled 10 V input to multiplier

Time constant = 100 ms, output multiplier x10

figures. The final choice of Q must be made as a compromise between the tolerable signal attenuation, impulse noise, noise DC offset and the drift with phase changes. For most of the flamespectral measurements made in this work, Q values of 2, 5, or 10 were used depending on specific conditions. A time constant of 100 ms was usually chosen for spectral scanning. This allowed a maximum scan rate of 2 resolution intervals per second (or $\sim 1 \text{ \AA s}^{-1}$ with maximum resolution).

The assumption has been made that when the mirror displacement is chosen as some fraction of the wavelength being measured, that this will be maintained when the wavelength is changed. The unimorph driving amplifier first reported cannot accomplish this feat but maintains a constant amplitude once set.⁴⁴ Thus, a programmable gain amplifier is required for SEMIDS.

In Figure 18, a schematic diagram is given for the programmable gain amplifier designed and built for SEMIDS. It was convenient to use the He-Ne laser line at 632.8 nm as the reference wavelength. This wavelength was assigned step number zero. As the grating is rotated to shorter wavelengths by incrementing the stepping motor, the number of steps taken is counted and converted to an analog signal to scale the mirror displacement. Because positive steps are taken to reach shorter wavelengths, the analog scaling is inverted and summed with an adjustable offset. Scaling of the mirror driving signal is done by multiplying the driving signal by the scaling factor prior to final amplification. The driving

Figure 18. Programmable gain amplifier.

CNTR is a Monsanto 106A Counter.

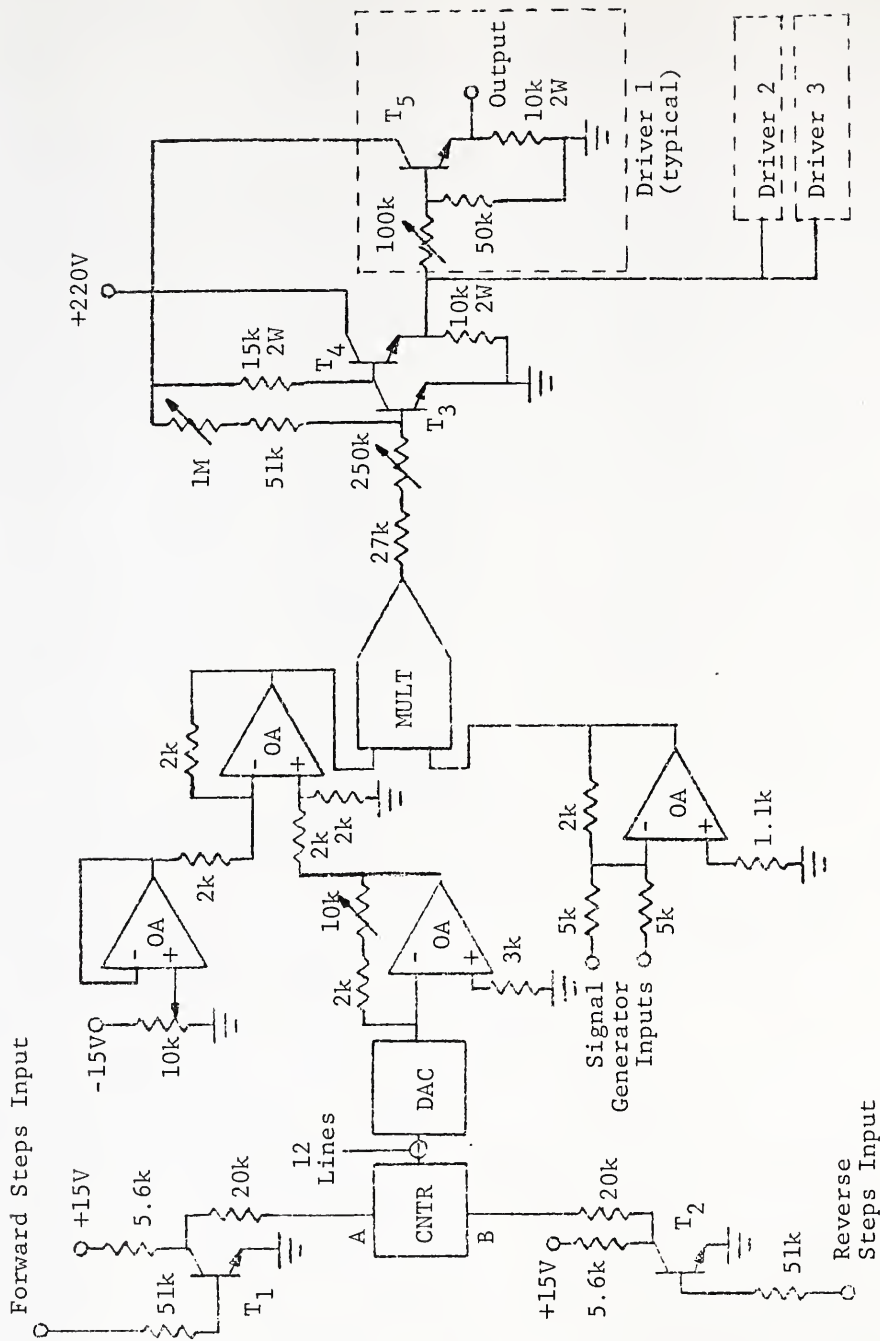
DAC is an Analog Devices MDA-L
Digital-to-Analog Converter.

OA is Operational Amplifier (741).

T_1 and T_2 are 2N3568.

T_3 , T_4 and T_5 are 2N3440.

All resistors are in ohms and are
1/2 W unless otherwise noted.



signal is obtained by summing the outputs of two signal generators each producing f_U or f_L of the desired frequency and waveform. The counter is a commercial stand-alone instrument with dual channel analog inputs and BCD outputs. It was used in the A-B mode (reversible counting).

The initial procedure was to set the wavelength drive to 632.8 nm, the counter to zero, and adjust the offset control to obtain a +10.00 V value for the scaling factor. Then the photomultiplier signal was observed with the oscilloscope for interference of the diffused laser beam. The output of each signal generator was adjusted to produce the desired displacements. The slope control was then set according to a calculation based on the number of steps required to change the wavelength to the Indium resonance line at 451.10 nm. This step number was found experimentally. This adjustment and the entire scaling process require linearity between wavelength and step number. The wavelength calibration plot shown in Figure 19 clearly demonstrates that the requirement is fulfilled.

Demodulation

This subject was touched in the last section. It is only brought up again here for completion.

The processing of the photo-current proceeds first by current to voltage conversion. The conversion ratio can be changed by decade from 10^4 to 10^8 volts per amp. Following this signal to the recorder, it is applied to a selective

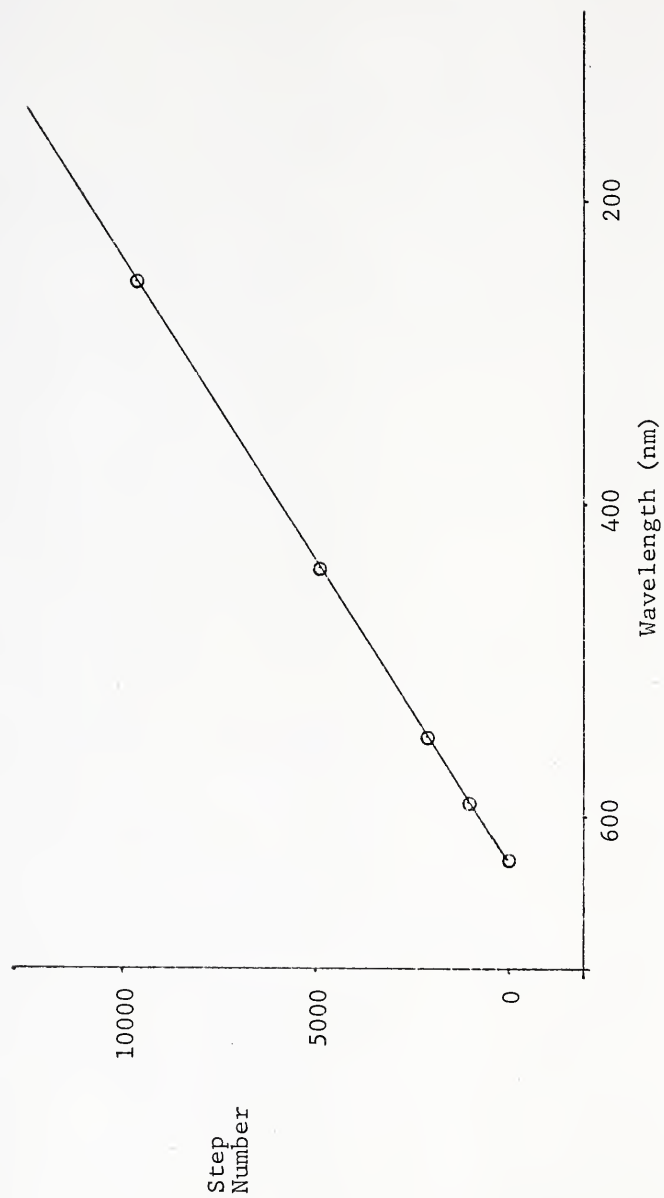


Figure 19. Wavelength calibration plot.

amplifier (or active bandpass filter) with adjustable Q, an AC amplifier, a multiplier/divider/low pass filter module used as a squaring circuit, a multiplier divider module used for square root and finally, the recorder.

The combination of squaring, low pass filtering, and then square rooting accomplishes the conversion of an AC signal to a DC voltage equal to the RMS AC voltage. However, problems were experienced with latch-up in the square root module. In order to prevent this, a sizable offset and an associated non-linearity had to be tolerated. A calibration was performed for the combined modules (DC output vs. true RMS input), and the curve is shown in Figure 20. All measurements reported in this thesis have been corrected to their true RMS values.

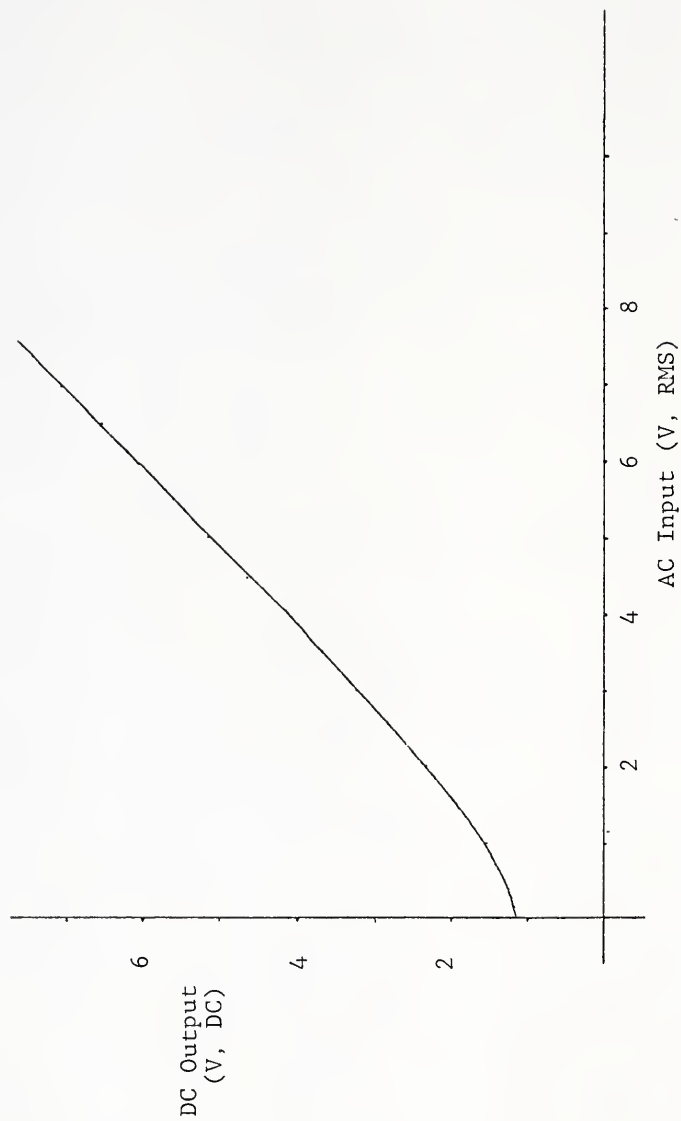


Figure 20. RMS calibration plot. DC output vs true RMS input.

CHAPTER IV SIGNALS, NOISES AND SIGNAL-TO-NOISE RATIOS IN SPECTROMETRY

The ultimate analytical potential of any technique depends upon its ability to collect information about an analyte with a high degree of accuracy and precision. When one technique is compared to another, both may be satisfactory for many situations. However, if the concentration of analyte is decreased, one technique usually proves to be more accurate and precise than the other at this lower concentration. Thus, the better technique may be able to make reliable analytical measurements in concentration ranges where competing techniques are useless.

One goal of analytical research is to develop new techniques and instrumentation with increased accuracy and precision as compared to existing analytical methods. This desire is twofold. First, these improvements directly affect the reliability of an analysis in a particular analyte concentration range. Second, these improvements extend the analyte concentration range over which reliable measurements can be made by lowering the limit of detection. This in itself is not important in many analyses routinely done in clinical laboratories or analytical testing laboratories since sufficient accuracy and precision already exist for the great

majority of analyses performed. In general, however, improvements, if not used to increase accuracy and precision, can be employed to decrease the total analysis time. But this may not be significant in techniques requiring a large expenditure of time in sample preparation. However, if the improved limit of detection of a new technique is significantly lower than in the standard technique, sample preparation can possibly be simplified since interfering species in the sample matrix may not need to be separated from the analyte but could simply be diluted (with the sample) to levels which cause no interference.

The repetitive occurrence of systematic errors in a procedure will lead to a wrong answer, even if the precision in obtaining this answer is very good. Thus, in considering accuracy and precision it is usually assumed that all systematic errors can be avoided by properly designing the measurement. Then, the accuracy is dependent only on the closeness of the mean value of the results obtained to the true value which is sought. The precision is an indication of the closeness of the results to each other and is usually expressed by their standard deviation.

A figure of merit for accuracy (assuming no systematic errors occur) and precision is the signal-to-noise ratio (S/N). This is defined as the ratio of the average result and the standard deviation of the individual results which were used in obtaining the average.

Signal and noise expressions for various spectrometric

methods were recently derived by Winefordner et al.⁵¹ This will be repeated here but only in sufficient depth to provide a background for a S/N model for SEMIDS. Two topics, whistle and spectral bandwidth considerations as pertaining to S/N, are presented here for the first time.

Signals

There are four basic methods for obtaining spectral information about an analyte.⁵¹ The conventional methods involve encoding the information in the time domain. The most fundamental method is the sequential-linear-scan (SLS) method in which a conventional single-slit dispersive spectrometer scans the wavelength range of interest at a uniform rate. If the spectral information desired is not also distributed uniformly over the chosen range, much time will be wasted as the spectrometer analyses regions containing no information. This can be avoided and the overall information gathering efficiency can be improved by programming the wavelength drive to slew as rapidly as possible from one spectral element of interest to the next one of interest while pausing only to make the desired measurements. This is the basis of the sequential-slewed-scan (SSS) method. The increased information gathering efficiency can be utilized either to increase the S/N or to decrease the total analysis time.

The information gathering efficiency can be further increased by eliminating scanning altogether and using a sep-

arate detector for each spectral component of interest. This multi-channel (MC) method is represented by direct reader type spectrometers and image detectors such as photographic emulsions and TV camera tubes.

Simultaneous detection of all spectral components of interest may be accomplished with a single detector if the spectral information is encoded in another data domain. This operation is called multiplexing and is the basis of the multiplex (MX) methods of spectral analysis. If multiplexing is performed with a Michelson interferometer, the data domain may be either the frequency domain (if constant mirror velocity is used) or the position of length domain (if the mirror is moved step-wise between fixed values of the path difference). A Fourier Transform is required to assemble the information in a domain where it can be interpreted. Thus MX spectrometry as a class is often called Fourier Transform Spectrometry (FTS). The abbreviation FTS is usually reserved for the small class within Fourier Transform Spectrometry utilizing the Michelson interferometer. However, multielement non-dispersive atomic fluorescence spectrometry is an equal member of this class.^{13,14,52-57} In Hadamard Transform Spectrometry (HTS), the data domain is the position of the multislit mask at the exit focal plane of the spectrometer. A Hadamard Transform is required to recover the spectral information. It can be shown that the same advantages and disadvantages of FTS also exist for HTS and for every other MX method. A systematic grouping of these methods is given in Table V.

TABLE V
SYSTEMATIC GROUPING OF MEASUREMENT METHODS

SPECTRAL DOMAIN	TIME DOMAIN	
	Sequential	Simultaneous
	<hr/>	
broad	Linear Scan (SLS)	Multiplex (MX)
<hr/>		
discrete	Slew Scan (SSS)	Multichannel (MC)
<hr/>		

When MX methods are compared with SLS, two potential advantages of MX emerge. First, the signals from every spectral component are analyzed all of the total analysis time in MX while only $1/N$ of the total analysis time is spent per component in SLS (where N is the total number of resolvable spectral components in the covered wavelength range). This represents an N -fold gain in signal gathering efficiency for MX vs. SLS and is due to the multiplex nature of the signals. This can eventually lead to an improvement in S/N which in the literature is usually called the multiplex advantage or Fellgett's advantage. A second advantage may be present depending on the specific instrumentation. Non-dispersive spectrometers (including the Michelson interferometer and its derivatives) can achieve high resolving powers while having a luminosity several orders of magnitude higher than conventional dispersive spectrometers. This corresponds to another gain in signal gathering efficiency. It is called the throughput advantage or Jacquinot's advantage. This is not always realized, however, as in the case of the single mask Hadamard Transform Spectrometer.

Some losses are expected, however, especially in the Michelson interferometer. A factor of 2 is always lost due to the modulation or chopping of steady state light levels by the interferometer. Another factor of 2 must be given up if a digital Fourier Transform is performed. Finally, the depth of modulation is not 100 % due to the imperfections in the optical components and their adjustments.

In considering signals and noises in spectrometry, it is most convenient to assume that photon counting detection can always be used and to derive all expressions in terms of the number of events counted in the analysis. The equations to be derived and the conclusions made from them are directly applicable to analog measurement systems.

To facilitate comparison of the various methods, it will be assumed that there exists a wavelength range with N resolvable components to be covered and that the resolving power for each technique is equal. Each of these components has a background count rate equal to R_{bi} when measured by either SLS, SSS, or MC. The peak count rate for MX is higher by the factor J due to the Jacquinot advantage. Within this spectral range is contained A spectral intervals with information which is desired. Each of these intervals has a signal count rate equal to R_{ai} as determined by either SLS, SSS, or MC. The peak signal count rate for MX is again higher by the factor J . All other spectral intervals are not important to the analytical determination but still contain background. It is also assumed that the total analysis time will be T regardless of the method chosen.

For SLS, each spectral interval is analyzed for a time equal to T/N . Thus, the number of counts obtained for u^{th} spectral component of interest is the product of the count rate and the time or $R_{au}T/N$.

For SSS, each spectral interval of interest is analyzed for a time equal to T/A . Thus, the number of counts obtained for the u^{th} interval is $R_{au}T/A$.

For MC, each spectral interval is analyzed all of the time. Thus, the number of counts obtained for the u^{th} spectral component of interest is $R_{au}T$.

For MX (based on the Michelson interferometer), the peak count rate is $J R_{au}$. However, this is modulated and then must be transformed, so a factor of 4 is lost. If the interferometer is otherwise perfect, the resultant number of counts obtained for the u^{th} spectral component of interest is $J R_{au}T/4$. All other multiplex methods yield similar results.

Noises

Noise in spectrometry will be divided into two classes:

- 1) noise proportional to the square root of the number of counts, and
- 2) noise proportional to the number of counts.

Shot noise (also called photon noise) is due to the quantum nature of light and due to the fact that light quanta arrive at a surface in a random fashion. Alternatively, emission of electrons from a photoemissive surface is a random process. Random events follow Poisson statistics which dictate that the standard deviation is proportional to the square root of the number of events. Shot noise is white in nature, i.e., there is no frequency dependence of the noise distribution (see Figure 21a). The shot noise is given by the square root of the total events observed, thus

$$N_s = \sqrt{Rt} \quad (30)$$

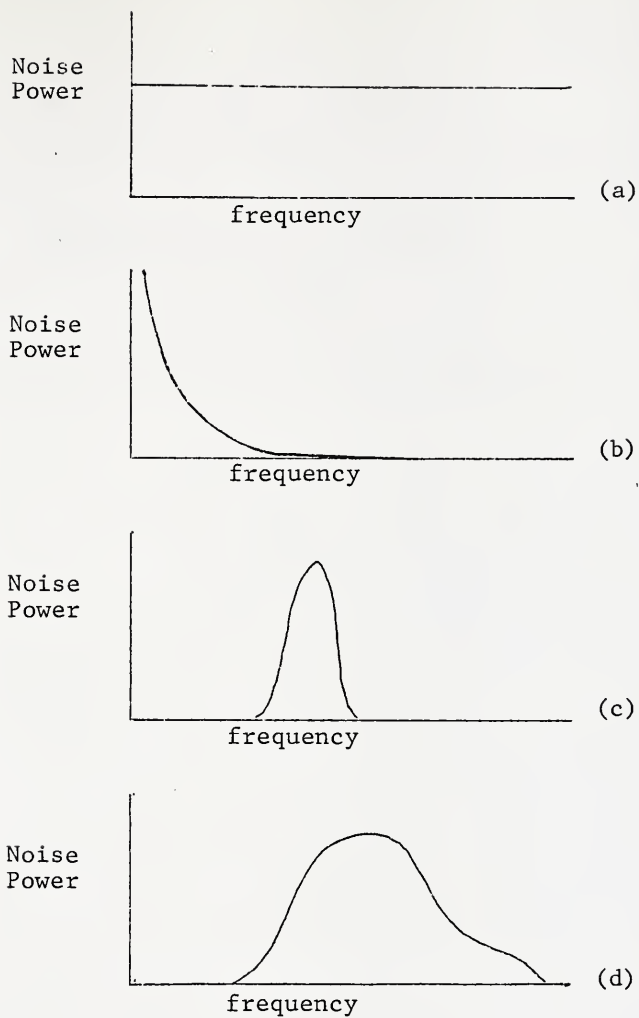


Figure 21. Noise power spectra. (a) White noise (shot). (b) $1/f$ noise (drift). (c) and (d) Oscillatory noise (whistle).

where N_s is the shot noise level, in counts, R is the counting rate of events, and t is the observation time.

All other noises encountered in spectrometry which are carried by light are proportional to the intensity of the light carriers. There are two main types which in this thesis are called drift and whistle.

Drift, also called fluctuation noise, $1/f$ noise, flicker noise, and pink noise, has been investigated by a number of workers.⁵⁸⁻⁶³ It is characterized by a noise power which is inversely proportional to the frequency and is negligible at high frequencies as is shown in Figure 21b. Drift is common in every sort of measurement system. The name flicker noise, is probably a misnomer because it implies an oscillatory phenomenon. This reflects a habit of workers in the field to lump many proportional noises into the same loosely defined category. In this paper, "drift" implies a $1/f$ character of the noise.

A general approach to quantitate a particular noise is to express the noise power as a function of frequency and integrate over the frequency limits imposed by the noise bandpass of the measurement system. The square root of the result is the noise which is detected. This was applied by Winefordner et al. to drift in digital form (for photon counting).⁵¹ The noise power spectral density is given by

$$N_d^2(f) = \frac{K_d^2 (Rt)^2}{f} \quad (31)$$

where K_d is a proportionality constant, R is the count rate

of the photon flux carrying the noise, t is the counting time, and $1/f$ is the noise power spectral distribution function. The total noise power measured is

$$N_d^2 = \int_{f_l}^{f_u} N_d^2(f) df = K^2 (Rt)^2 \ln \frac{f_u}{f_l} \quad (32)$$

where f_l and f_u are the lower and upper noise cutoff frequencies of the measurement system assuming a rectangular bandpass. Setting

$$K^2 \ln \frac{f_u}{f_l} = \xi_d^2 \quad (33)$$

results in $N_d = \xi_d Rt$. ξ_d is a proportionality constant which will be called the drift factor.

Whistle noise has not been previously treated in the literature except for noises which have been called interference noise.⁶⁴ This was usually associated with such noise sources as inductive line frequency pick-up of AC ripple on the output of AC powered light sources. Noise from flicker of light filaments has previously been loosely cast with drift. However, such noise is generally not $1/f$ in nature. Another important noise source in flame spectrometry is flame flicker which also was previously lumped with drift. It is the intent of this section to create an awareness in the reader of the difference between genuine drift ($1/f$ in nature) and genuine oscillations (centered about some frequency). Noise power spectra of whistle noises are shown in Figures 21c and d.

The name "whistle" stems from the fact that these noises are caused by physical oscillations which also create audible

noise. It is interesting to note that for the flame noise spectra recently appearing in an article by Talmi, Crosman and Larson, the flames exhibiting the greatest (non-white) audio frequency optical noise components are also the same ones which produce the greatest audible noises.⁶⁵ Work is in progress in this laboratory to correlate audio noise from flames (detected with a microphone) with the noise observed on the light signal.

Published noise spectra show whistle varying in both frequency and bandwidth.^{59,63,65,66} The (audibly) quiet laminar flames have little whistle, mainly of low frequency and narrow frequency bandwidth. Noise spectra of turbulent flames exhibit large broad bands of whistle noise extending up to the cut-off frequency used with the spectrum analyzer (which was about 5 kHz).⁶⁵

The quantitative approach which was applied to drift may be applied to whistle. However, difficulty arises in deciding on a suitable noise power spectral distribution. A Gaussian distribution or a sum of Gaussian peaks may be assumed, but this leads to more difficulty since the Gaussian function is difficult to integrate. General trends can be established by assuming a rectangular frequency distribution. This is not a bad assumption for use in choosing measurement parameters if the rectangle is purposely chosen to be too big. Let the distribution function be

$$N_P(f) = \begin{cases} 1 & f_a \leq f \leq f_b \\ 0 & f < f_a, f_b < f \end{cases} \quad (34)$$

as is shown in Figure 22. Following the previous procedure, it is found that

$$N_w^2 = K_w^2 (Rt)^2 \int_{f_\ell}^{f_u} N_p(f) df. \quad (35)$$

Four situations exist in evaluating the integral:

- 1) If $f_\ell, f_u < f_a$ or $f_b < f_\ell, f_u$, then the integral is zero and no whistle noise power is detected.
- 2) If $f_a < f_\ell < f_u < f_b$, then the whistle noise power detected is proportional to the bandwidth of the detection system, $\Delta f = f_u - f_\ell$.
- 3) If $f_\ell < f_a, f_b < f_u$, then the whistle noise power detected is independent of Δf .
- 4) If $f_\ell < f_a < f_u < f_b$ or $f_a < f_\ell < f_b < f_u$, then the whistle noise power detected depends on the overlap of $f_b - f_a$ with Δf .

Clearly, the only favorable condition is the first, and this justifies the choice of the rectangular frequency distribution for observing the trend. Thus, to minimize the detected whistle noise, the measurement (electronic) bandpass must be positioned in a region of the frequency spectrum which is minimized in whistle noise.

When whistle noise can not be eliminated, it is treated as a proportional noise by setting

$$K_w^2 \int_{f_\ell}^{f_u} N_p(f) df = \xi_w^2 \quad (36)$$

which leads to $N_w = \xi_w Rt$. ξ_w is called the whistle factor and is analogous to ξ_d .

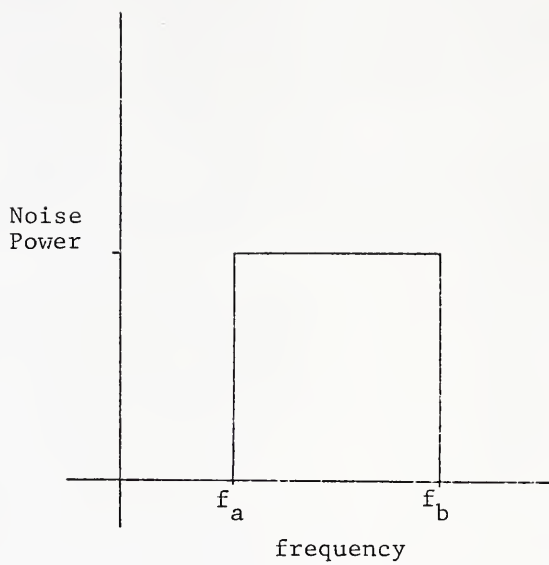


Figure 22. Rectangular frequency distribution assumed for whistle.

It has not been the habit of workers to do so, but it is absolutely necessary to give an estimate of the total counts observed and the effective measurement cut-off frequencies before any noise spectra from different workers can be compared because the ratio of shot noise to other (proportional) noises changes with these parameters. Thus, for very low light levels, shot noise will be the limiting noise over nearly all of the frequency spectrum except perhaps for the lowest frequencies (up to 1 Hz) where drift ($1/f$ noise) will predominate. Alternatively, at high light levels, whistle noise will rule much of the frequency spectrum.

Noise Sources

Noises are listed by source in Table VI.

Detector noise. Shot noise due to thermionic emission from the photocathode and the first dynode is the overwhelming detector noise for photomultiplier tubes operated at room temperature. Drift in the applied voltage can induce gain drift in the tube and thus create a $1/f$ type detector noise but only in analog measurement circuitry. With photon counting, drift errors are minimized and also the dark signal level can be minimized by ignoring thermionic emission from the dynodes via pulse height discrimination.

Signal carried noises. Drift and whistle noises originating in the light source for absorption or fluorescence measurements are carried by the signal. Analyte concentration fluctuation noise is also carried by the signal. A shot

TABLE VI
GENERAL SIGNAL AND NOISE TERMS IN SPECTROMETRY

Method	Signal	Detector	Shot Noise		Drift		Whistle	
			Signal	Background	Signal	Background	Signal	Background
SLS	$R_{au} T/N$	$\sqrt{R_D} T/N$	$\sqrt{R_{au}} T/N$	$\sqrt{R_{bu}} T/N$	$\xi_{ds} R_{au} T/N$	$\xi_{db} R_{bu} T/N$	$\xi_{ws} R_{au} T/N$	$\xi_{wb} R_{bu} T/N$
SSS	$R_{au} T/A$	$\sqrt{R_D} T/A$	$\sqrt{R_{au}} T/A$	$\sqrt{R_{bu}} T/A$	$\xi_{ds} R_{au} T/A$	$\xi_{db} R_{bu} T/A$	$\xi_{ws} R_{au} T/A$	$\xi_{wb} R_{bu} T/A$
MC	$R_{au} T$	$\sqrt{R_D} T$	$\sqrt{R_{au}} T$	$\sqrt{R_{bu}} T$	$\xi_{ds} R_{au} T$	$\xi_{db} R_{bu} T$	$\xi_{ws} R_{au} T$	$\xi_{wb} R_{bu} T$
MX	$JR_{au} T/4$	$\sqrt{R_D} T$	$\sqrt{\frac{JT}{4}} \sum_{j=1}^A R_{aj}$	$\sqrt{\frac{JT}{4}} \sum_{i=1}^N R_{bi}$	$\xi_{ds} \frac{JT}{4} \sum_{j=1}^A R_{aj}$	$\xi_{db} \frac{JT}{4} \sum_{i=1}^N R_{bi}$	$\xi_{ws} \frac{JT}{4} \sum_{j=1}^A R_{aj}$	$\xi_{wb} \frac{JT}{4} \sum_{i=1}^N R_{bi}$

noise level is associated with the total signal level and measurement duration.

Background carried noises. Other shot noise, drift and whistle may exist and may not be carried by the signal but may be carried by stray light originating in the background of a line source, such as a hollow cathode lamp, or a continuum source, or in the sample cell, such as background or solvent fluorescence, flame emission and flame fluorescence.

Total noise. Total noise is obtained by first adding the statistically dependent noises together to form a set of statistically independent noises. The independent noises are then summed quadratically to give the total noise

$$N_T = \sqrt{N_a^2 + N_b^2 + \dots} \quad , \quad (37)$$

where a, b, etc. are independent noise sources. For example, drift among the various spectral components in the background light is considered dependent. The same is assumed for whistle in the background light and for drift and whistle in the various signal spectral components. However, each of these sums is considered independent. Some statistical dependence must exist between the frequency-dependent noises, especially between the signal and background whistle, but the extent is not known. The assumption of independence does not lead to any serious errors unless any two proportional noises are nearly equal and are dominating the total noise.

Signal-to-Noise Ratios

SLS, SSS, and MC. In each of these methods, one spectral component is measured independently of the others. The signal and noise expressions come directly from the previous discussion and are tabulated in Table VI. The total noise is the quadratic sum of the noises shown for each method.

MX. Because all spectral components are measured simultaneously, the spectral dependence of the noises must be considered. The total noise may be analysed as follows. The detector noise is identical to the cases above. The light carried shot noise, N_S , equals the square root of the total count for all signal and background components or

$$N_S = \sqrt{\frac{JT}{4} \left(\sum_j R_{aj} + \sum_i R_{bi} \right)} . \quad (38)$$

Drift noises among various signals are assumed dependent and add linearly. An exception to this assumption is multielement atomic absorption or fluorescence utilizing separate sources for each element. Then, drift originating in the sources is independent but drift originating in the flame or nebulizer is dependent. Because drift in a source can be easily minimized (by double beam optics) while drift in the sample (i.e., the flame) can not, the assumption of the dependence of these drifts is not a bad one. The total signal drift noise, N_{ds} , is

$$N_{ds} = \xi_{ds} \sqrt{\frac{JT}{4} \sum_j R_{aj}} . \quad (39)$$

Similarly, signal whistle noise, N_{ws} , and background drift, N_{db} , and whistle, N_{wb} , noises add linearly over the spectral distribution. The results are

$$N_{ws} = \xi_{ws} \frac{JT}{4} \sum_j R_{aj} \quad (40)$$

$$N_{db} = \xi_{db} \frac{JT}{4} \sum_i R_{bi} \quad (41)$$

and

$$N_{wb} = \xi_{wb} \frac{JT}{4} \sum_i R_{bi} . \quad (42)$$

The various drift and whistle factors are distinguished by their subscripts and their values depend on the parameters of the measurement system. The total noise is the quadratic sum of these noise components. The use of Table VI is contingent on the ability to distinguish the u^{th} sample spectral component from the u^{th} background spectral component. If R_{bu} is very small compared to R_{au} , or if the signal is modulated and the duty cycle, the ratio of the signal "on" time to the total analysis time, is reflected in the value of R_{au} , the table may be used as it stands. Otherwise, a separate background measurement must be made, and then the signal is the difference of the two results, and the noise is the quadratic sum of the total noises of the two measurements.

Examination of Table VI leads to several conclusions with respect to S/N of the various methods.^{14,51,67-69}

- 1) When detector noise is the limiting noise, the largest S/N exists for MX if J is greater than 4. This is the

typical situation in the infrared spectral region and reflects the growing popularity of MX instrumentation for that region.

- 2) When signal or background carried shot noise is the limiting noise, S/N for MX may be better than the other methods for the stronger signal components and worse for the weaker ones. Because analytical measurements are often required of weak spectral components, this represents a multiplex disadvantage. This has been treated in detail in the literature.⁶⁷⁻⁶⁹
- 3) When signal carried drift or whistle is the limiting noise, MX methods are generally worse than in case 2.
- 4) When background carried drift or whistle is the limiting noise, MX methods may be even worse than in case 3.
- 5) MC is always better than SSS which is always better than SLS. When the fraction of components measured, A/N, is small, the SSS results approach MC. When A/N approaches unity, SSS approaches SLS.

Modulation

Noises which may be reduced (relative to the signal) by signal modulation are called additive noises. Drift and whistle noises are additive. Shot noise may not be reduced by signal modulation and is a multiplicative noise.

For example, modulating the source in flame atomic absorption can reduce the flame background drift and whistle.

Double beam optics can reduce the drift and whistle noise in the light source.

In general, any frequency-dependent noise which originates after the modulation step can be reduced. However, for single beam optics, signal carried noises are also modulated. When this occurs, these noises are translated from their own frequencies to the modulation frequency region. Demodulation not only recovers the signal but also recovers the signal carried noise.

Simple modulation (chopping) requires that the signal must be reduced. If modulation is successful, the total noise attenuation is greater than the signal attenuation so that there is a net increase in S/N. When modulated (as with a rotary chopper), all signals become the product of the original signal and the duty cycle of the modulation, D . Signal carried shot noise is reduced by \sqrt{D} . Signal carried proportional noises are reduced by D . Thus, if signal carried shot noise is the limiting noise, modulation reduces the S/N by \sqrt{D} . If signal carried proportional noise is the limiting noise, modulation does not change S/N.

Background carried drift is reduced for another reason. Recall that $\xi_d^2 = K_d^2 \ln(f_u/f_\ell)$. For DC detection, the lower frequency, f_ℓ , is determined by the frequency at which a complete series of measurements is made, i.e., blank, sample, and standard, and f_u is determined by the time constant, τ , of the measurement system and is approximately equal to $1/4\tau$. When the signal is modulated, the noise bandwidth for additive

noise which is not modulated is shifted to the modulation frequency region and is given approximately by $f_m \pm f_u$ where f_m is the modulation frequency. Thus

$$f'_u = f_m + f_u$$

and

$$f'_\ell = f_m - f_u.$$

If f_m is large compared to f_u , the ratio f'_u/f'_ℓ is nearly unity and is very much lower than f_u/f_ℓ . Thus,

$$\xi'_d = \sqrt{K_d^2} \ln \frac{f'_u}{f'_\ell}$$

can be greatly lowered compared to ξ_d which lowers the detected drift noise by the same factor.

Whistle noise does not present a problem for DC detection systems because it is usually not significant at lower frequencies when compared to drift noise. However, if modulation is used to reduce drift, but f_m is poorly chosen and is in a region with strong whistle, the total noise could be increased. Thus, f_m must be carefully chosen to be in a region which is relatively free from whistle noise to minimize the integral in Equation 36 which also minimizes ξ_w .

It has already been stated that source modulation will not reduce noise from analyte fluctuations. The only method by which this can be accomplished is sample modulation. Analytical DC measurements are actually not DC but are AC at very low frequencies due to sample modulation. Consider what will occur if the periodic checking of standards is neglected. f_ℓ tends to zero, thus $\ln (f_u/f_\ell)$ and drift noise tends to

infinity. Accuracy is completely lost due to the drift but precision could be determined by other noises and may be quite good over short time intervals. Serious errors could be made with apparently good S/N. The long term drift, when considered over a short time interval, behaves like a determinate error.

With sample modulation, f_{ℓ} is still determined by the frequency of performing a complete measurement, i.e. sample, standard and blank and f_u is still determined by the electronic time constant. Thus, if the sampling apparatus is common for all three test solutions (sample, standard, and blank) such that drift (especially nebulization drift) affects each measurement exactly the same, then drift of the signals is compensated by periodic ratioing of the sample and standard. Drift in the background is eliminated by periodic subtraction of the blank from both the sample and standard. Whistle is eliminated by the proper choice of f_{ℓ} .

This points out the necessity of new research in the area of high speed sample modulation.

Spectral Bandwidth Considerations

In comparing S/N for various spectral measurement methods, the first assumption usually made is that the resolving power is the same for each method. This invariably leads to a large Jacquinot advantage for MX because very small slit widths must be used in conventional dispersive spectrometers to achieve the resolving power of a typical interferometer. However, this

is not necessarily so. Consider resonance fluorescence of an element excited by a perfect line source. Modulation of this source results in a modulated fluorescence signal. Any emission from another element at a slightly different wavelength is not modulated. Because this emission can be distinguished from the desired signal, the effective resolution of the complete instrument is the width of the atomic line regardless of the spectral bandpass of the spectrometer. However, any spectral component striking the detector can carry noise. The total noise will be dependent on the presence of all radiation reaching the detector and any noise carried by it and therefore will depend on the spectral bandpass of the spectrometer. Thus, as is demonstrated here, the spectral bandpass of the signal may be different than the spectral bandpass of the noise.

An interesting consequence results from this concept. Consider a modulated atomic line with a white light DC background measured by a conventional dispersive spectrometer. If the modulation frequency is properly chosen, the limiting noise will be shot noise on the signal for small values of the slit width.

Because the signal measured from narrow line sources is proportional to the slit width, and because the shot noise is proportional to the square root of the signal (and the square root of the slit width) a plot of the $\log S/N$ vs. \log (slit width) will have a slope of 0.5. However, the intensity of the white light background increases with the

square of the slit width. Shot noise from the background must be increasing linearly with the slit width. A point must be reached when the background shot noise exceeds the signal shot noise and then dominates the total noise. When this occurs, S/N has reached a constant value, and the slope of the log/log plot above becomes zero. Alternatively, proportional signal carried noise may become dominant. This also gives a slope equalling zero. Further increases in the slit width will not increase S/N but, when background carried proportional noise ultimately becomes dominant, S/N will decrease, and the slope will be -1. This behavior is shown in Figure 23.

From shot noise alone, it can be argued that MX methods, in this case, must be inferior to the conventional spectrometric methods if the increase in the spectral bandwidth observed by the detector is greater than the increase in throughput. In addition, the choice of a white light background is a poor one. All flames have band emission from various species such as OH, CH, CN, etc., which will further increase the shot noise in MX but which can be rejected in the conventional dispersive spectrometer by the proper choice of the slit width (or spectral bandpass). In addition to the flame background species, many elements form oxides and hydroxides in flames which are considered useless for quantitative analysis due to their bandwidths, but which have bright emission over broad spectral regions. This is still another noise source for MX which is easily rejected by conventional instrumentation.

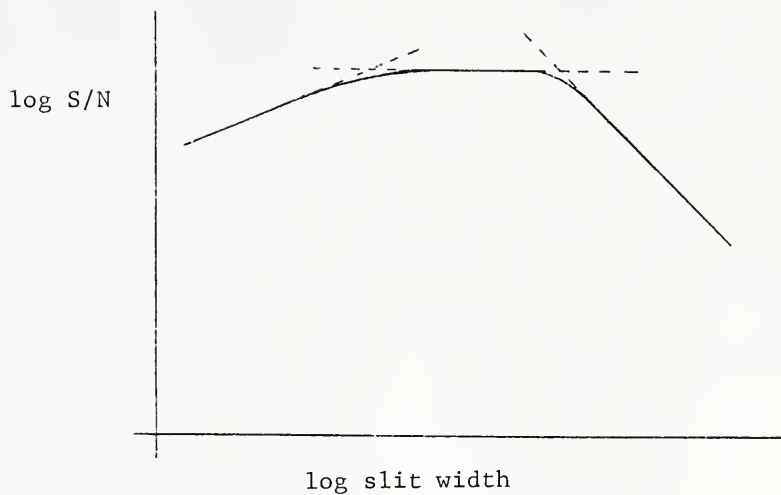


Figure 23. Theoretical dependence of S/N on slit width for the measurement of a line against a white light background.

If a continuum source is used to excite the fluorescence in the example above, things are now a little different. The spectrometer bandpass must be chosen such that the line of interest is sorted from any others which may be near it. Once this is done, the signal can still be distinguished from DC emission within the spectrometer bandwidth, so the spectral bandwidth of the signal is still the width of the atomic line. For nearly all elements (considered present together in one sample), the flame background shot noise limit still applies near the limit of detection.

Flame background fluorescence can not be distinguished from atomic fluorescence except by spectral (rather than electronic) discrimination. When this is appreciable or when signals are not modulated, as in atomic emission, the signal spectral bandwidth and the noise spectral bandwidth are both determined by the slit width.

The obvious conclusion which can be drawn from these observations is that any S/N limited by shot noise from a continuum background can not be improved by a throughput advantage derived from an increase in the spectral bandwidth controlling the noise. The only possible advantage results from a throughput increase accomplished by increasing the solid angle collected.

CHAPTER V THE SIGNAL-TO-NOISE RATIO FOR SEMIDS

The techniques of signal and noise analysis described in Chapter IV can be applied to specific instrumentation. This will be done here for SEMIDS to yield a useful S/N behavior model. With this model, areas of greatest potential usefulness and areas of complete failure can be predicted.

Signal

Equation 29 gives the intensity expression for SEMIDS for the double modulation technique which was used experimentally. When X_L and X_U are $\lambda/4$, half of the signal power resides in the vicinity of f_U while the other half is in the vicinity of $2f_U$ in the frequency spectrum. Since only one of these frequency regions is monitored, i.e., since the selective amplifier can only be tuned to f_U or $2f_U$ but not to both, half of the signal is lost. Additionally, another factor of 2 is lost due to the modulation of the signal. If R_{au} is the photon count rate of a signal in a conventional spectrometer (SSS), then the signal, S , for SEMIDS in digital form is

$$S = \frac{JR_{au}T}{4} , \quad (43)$$

where J is the (geometric) throughput increase of Jacquinot factor for SEMIDS as compared to the conventional spectrometer and T is the total analysis time.

Noise

Again, noise is most easily listed by the sources.

Detector noise. Detector contributed shot noise is identical to that in the previous cases (Chapter IV).

Signal carried noise. The signal carried shot noise equals the square root of the total number of signal counts observed in a measurement period. Signal carried drift and whistle noises are directly proportional to the signal with proportionality constants ξ_{ds} and ξ_{ws} as before.

Background carried noise. The background contribution from the mirror is very different from that of the grating due to the dispersion of light from the latter.

The spectral bandwidth of the grating arm contribution can be found by ignoring the mirror and beamsplitter altogether and by treating what is left as a spectrometer. Thus

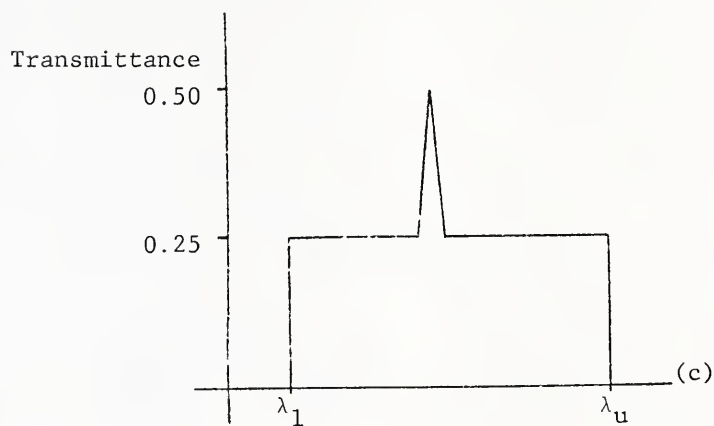
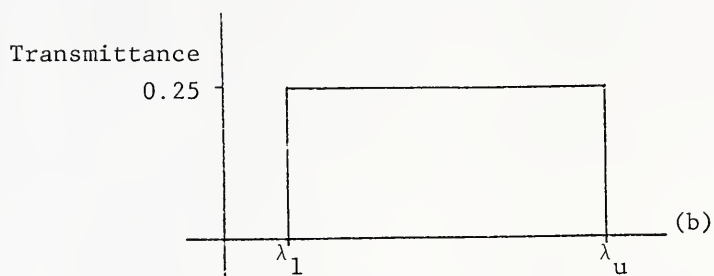
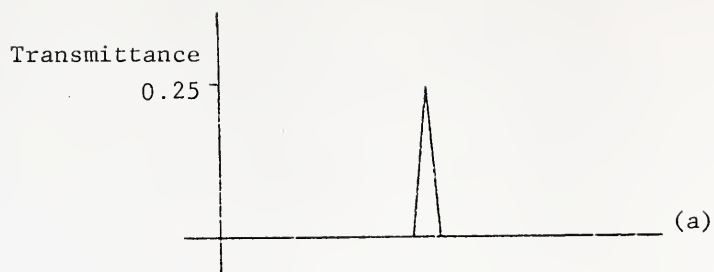
$$\Delta\lambda = \frac{w}{f} d \cos \theta , \quad (44)$$

where $\Delta\lambda$ is the spectral bandwidth (halfwidth) of the emergent light, w is the width of the apertures (assuming the entrance and exit apertures are equal), f is the focal length of the collimator and focusing lenses (assuming they are identical), d is the groove spacing on the grating and θ ($= \arcsin(\lambda/2d)$) is the grating angle. Equation 44 applies directly only when rectangular slits are used in a spectrometer. However, for the purpose at hand, no serious error is encountered by the application of this equation to SEMIDS which uses circular apertures. Thus, the background light contributed from the grating will be assumed to follow a triangular spectrometer function with a bandwidth equal to $\Delta\lambda$. Let it further be assumed that the center wavelength is not attenuated except by the two interactions with the beamsplitter. Thus, the peak transmittance is 0.25 as shown in Figure 24a.

The background contribution from the mirror arm is not dispersed and thus covers the entire optical spectrum. For convenience, it is assumed that the detector spectral response is rectangular with a sharp upper response cutoff at λ_u and a sharp lower response cutoff at λ_l as is shown in Figure 24b. The only attenuation is due to the beamsplitter and the instrument transmittance for this arm is 0.25 over the entire spectrum.

Except for the signal wavelength at which interference occurs, the total background is found by summing the two contributions. The result is shown in Figure 24c.

Figure 24. (a) Grating contribution to the white light background transmittance. (b) Mirror contribution. (c) Total.



The reciprocal linear dispersion for the grating and lens combination in SEMIDS is 8.34 nm/mm. Thus, the bandwidth for 5 mm apertures is 41.7 nm for the grating contributed background.

The response bandwidth of the photomultiplier tube used is about 500 nm. Thus, for a white light background, it is doubtful if the grating arm contribution to the total background could ever be significant. Nevertheless, those contributions will be considered.

The number of background photons for the i th spectral component reaching the detector in the period T which is contributed from the mirror arm is $JR_{bi}T/4$ where R_{bi} is the photon count rate for that component with a dispersive spectrometer. The total number of background counts contributed by the mirror arm, C_{bm} , is found by summing over the number of spectral components (spectral resolution intervals), N , in the spectrum,

$$C_{bm} = \sum_{i=1}^N \frac{JR_{bi}T}{4} \quad (45)$$

The contribution to the observed background from the grating is identical except that it is modified by dispersion. The correct contribution results when Equation 45 is multiplied by the spectrometer function of a spectrometer employing the same grating, collimating and focusing elements and apertures as SEMIDS. If this function is $S(\lambda)$, which equals 1 for the center wavelength of the spectrometer bandpass, ranges between 0 and 1 for other wavelengths within the bandpass and equals

0 for all wavelengths not within the bandpass, then the grating arm contribution to the observed background, C_{bg} , is

$$C_{bg} = S(\lambda) \sum_{i=1}^N \frac{J R_{bi} T}{4} .$$

If $S(\lambda)$ is replaced by its value, S_i , for every wavelength component then

$$C_{bg} = \sum_{i=1}^N \frac{S_i J R_{bi} T}{4} . \quad (46)$$

The total number of background counts observed, C_{bt} , is the sum of the mirror and grating contributions,

$$C_{bt} = \sum_{i=1}^N \frac{(S_i + 1) J R_{bi} T}{4} . \quad (47)$$

In most real situations (and especially with flame or plasma sources), the S_i contribution will be negligible. For the purpose of establishing trends, no serious error is ever encountered by ignoring S_i .

The background carried shot noise is the square root of the total number of background counts observed in the measurement period. The background carried drift and whistle noises are proportional to the number of background counts observed. The proportionality constants are ξ_{db} and ξ_{wb} .

The various noise components for SEMIDS are listed in Table VII. The total noise is the quadratic sum of the statistically independent noise components listed in the table.

The measurement of only one signal component will be considered. Therefore, for comparison with other methods,

TABLE VII
NOISE COMPONENTS IN SEMIDS

Source	Noise Type	Noise Term
Detector	Shot	$\sqrt{R_D T}$
Signal	Shot	$\sqrt{\frac{JR_{au} T}{4}}$
	Drift	$\xi_{ds} \frac{JR_{au} T}{4}$
	Whistle	$\xi_{ws} \frac{JR_{au} T}{4}$
Background	Shot	$\sqrt{\sum_{i=1}^N (S_i + 1) \frac{JR_{bi} T}{4}}$
	Drift	$\sum_{i=1}^N \xi_{db} (S_i + 1) \frac{JR_{bi} T}{4}$
	Whistle	$\sum_{i=1}^N \xi_{wb} (S_i + 1) \frac{JR_{bi} T}{4}$

the factor A in Table VI should equal 1. Also note that the background may contain other signal components which are not currently being measured.

Signal-to-Noise Ratio for SEMIDS

The S/N for the SSS method and for SEMIDS for the analysis of a single spectral signal are given in Table VIII. Comparison of these ratios yields predictions of the potential applicability of SEMIDS as a replacement for the more conventional technique.

There are two possible advantages for using SEMIDS. First, the signal is larger than for SSS if the factor J is greater than 4. J is typically 10^2 to 10^3 and thus a substantial improvement in signal gathering efficiency can be realized. Second, the factor ξ_{db} is significantly reduced in SEMIDS due to the signal modulation. Therefore, in situations where background drift noise is of major importance, SEMIDS could offer substantial noise reduction. However, it must be emphasized that the background light flux is so greatly increased due to the non-dispersed mirror arm contribution over that of the typical background observed in SSS that whistle noise, which is usually not significant with DC detection systems relative to the observed drift noise, is greatly increased.

The S/N behavior of SEMIDS was investigated experimentally for flame atomic emission. An Ar-separated air/acetylene flame was used. This flame was chosen for its combination of good

TABLE VIII
COMPARISON OF S/N FOR SSS AND SEMIDS FOR THE
MEASUREMENT OF ONE SPECTRAL SIGNAL

$$(S/N)_{\text{SSS}} = \frac{R_{\text{au}} T}{\sqrt{R_{\text{D}} T + R_{\text{au}} T + R_{\text{bu}} T + (\xi_{\text{ds}} R_{\text{au}} T)^2 + (\xi_{\text{ws}} R_{\text{au}} T)^2 + (\xi_{\text{db}} R_{\text{bu}} T)^2 + (\xi_{\text{wb}} R_{\text{bu}} T)^2}}$$

$$(S/N)_{\text{SEMIDS}} =$$

$$\frac{JR_{\text{au}} T}{4} + \frac{JR_{\text{bi}} T}{4} + \frac{JR_{\text{au}} T}{4} + (\xi_{\text{ds}} \frac{JR_{\text{au}} T}{4})^2 + (\xi_{\text{ws}} \frac{JR_{\text{au}} T}{4})^2 + \left\{ \sum_{i=1}^N (\xi_{\text{db}} (S_i + 1) \frac{JR_{\text{bi}} T}{4})^2 + \right.$$

$$\left. + \left\{ \sum_{i=1}^N (\xi_{\text{wb}} (S_i + 1) \frac{JR_{\text{bi}} T}{4})^2 \right\} \right\}$$

atomization efficiency for most elements and its relatively low background. Details of the burner, flame and external optics are given in Table IX. It was found in all cases except for extremely large signals that the limiting noise was carried on the background light. In some cases, much of this background light was due to emission from other lines and bands of the analyte element at wavelengths other than the one being measured. This was extreme for Ca and Sr due to the very strong emission bands of CaOH and SrOH. However, for every other element near its limit of detection, the limiting noise was due to flame background. The elements investigated were Na, Ca, Sr, Li, Au, Cu, In, Cr, Mg, Ni, and Cd.

Initially, the existence of whistle noise had not been considered. Because background drift is virtually eliminated by the signal modulation, it was expected that the background carried limiting noise would be shot noise. An experiment was performed to verify this. The experimental design was to measure the flame background noise, then attenuate the flame background light flux with a neutral density filter and observe the changes in the noise (see Appendix). A square root dependence of the noise on the light flux indicates shot noise character.

An Ealing ND 1.0 filter was used (#26-5777, Ealing Corporation, South Natick, Mass.). The transmittance of this filter (averaged over the entire flame background spectrum as observed by the detector) was found by experiment to be

TABLE IX
BURNER, FLAME AND EXTERNAL OPTICS USED
FOR FLAME EMISSION MEASUREMENTS

Burner	Model 290-010	Perkin Elmer Corp. Norwalk, CO.
Nebulizer	Model 303-0352	Perkin Elmer Corp. Norwalk, CO
Capillary Burner Head Flame Separator		Laboratory Con- structed
Lens	2 inch diameter 2 inch focal length Spectrosil	Esco Optics Oak Ridge, N. J.

Flame Gas Flow Rates:

C_2H_2 1.5 l min⁻¹

Air 9.7 l min⁻¹

Ar 15.5 l min⁻¹

Solution Flow Rate 5 ml min⁻¹

0.106. This corresponds to an attenuation factor ($1/T$) of 9.41. This experiment is outlined in the Appendix. The details are given in Table X. The results indicate primarily proportional noise character and inspired the theoretical considerations which have been made for whistle noise.

The conclusion of whistle noise dominance on the flame background light for SEMIDS can also be made from theory once the existence of whistle noise is assumed. Compare the background shot and whistle noise terms in the total noise expression, i.e., the squares of the terms in Table VII. For $\xi_{wb} = 10^{-3}$, $N = 10^4$, $J = 10^2$, $T = 1$ s and neglecting S_i , a background count rate, R_{bi} , of only 4 s^{-1} per spectral resolution interval (measured by SSS) equates the two noise terms for SEMIDS. An average background count rate much lower than this would be necessary to make the background whistle noise negligible with respect to the background shot noise. A much higher count rate would mean that shot noise is negligibly small compared to whistle noise. For example, if the average background count rate is 40 s^{-1} , the square of the whistle noise would be a factor of 10 larger than the square of the shot noise.

The background count rate observed for the flame used typically ranges across the uv-visible spectrum from 5 to 700 s^{-1} with an average value of about 300 s^{-1} (as measured by SSS). The details of this measurement are given in Table XI. Thus, it is doubtful that shot noise could ever be important in SEMIDS.

TABLE X
FLAME BACKGROUND NOISE CHARACTERIZATION
FOR SEMIDS

Ar Separated C_2H_2 /air flame (see Table IX)

Entrance Aperture = Exit Aperture = 5 mm

650 V DC applied to PM Tube

Transconductance = 10^7

Selective Amplifier:

Frequency = 2 kHz

Q = 2

Gain = 10

AC Amplifier Gain = 20

Multiplier:

10 V AC Input

Time Constant = 1 s

Output x 10

Recorder Span = 10 mV (x100 attenuator)

Total Noise (no optical attenuation) = 1.93 V rms

Noise measured with attenuator = 0.233 V rms

Calculated Shot Noise = 0.358 V rms

Calculated Proportional Noise = 1.90 V rms

TABLE XI
SSS BACKGROUND COUNT RATES OF THE
AR SEPARATED C_2H_2 /AIR FLAME

Monochromator, grating, photomultiplier tube
and photon counter used are the same compo-
nents listed in reference 70.

Slit Height = 10 mm

Slit Width = 10 μ m

Resolution = 1.2 Å (Manufacturer's figure for
the grating and slit width
used)

Flame (see Table IX)

Results:

Wavelength, nm	Count Rate, s^{-1} *
200	5
250	25
300	130
350	220
400	350
500	650
600	175

* These figures are corrected for a 20 s^{-1}
dark count rate.

A typical analytical situation might yield a S/N limited by background shot noise with the SSS method. If the same measurement is made with SEMIDS, background whistle noise limitation is most likely. If the background is uniform throughout the spectrum and if S_i is neglected, the ratio of the S/N for the two techniques is

$$\frac{(S/N)_{\text{SEMIDS}}}{(S/N)_{\text{SSS}}} = \frac{1}{\xi_{\text{wb}} N R_{\text{bi}} T} \quad (48)$$

Thus, for the values of ξ_{wb} , N and T assumed above, SEMIDS has no chance for improving the S/N.

When background carried noise limits the S/N in SEMIDS, conditions may be improved by limiting the bandwidth of this background with a filter. This is demonstrated experimentally in Figure 25. The first trace is the signal for the flame emission of a 0.1 ppm Na solution. The second trace was obtained for the same solution but with an interference filter (589 nm, 8 nm bandpass, Bausch and Lomb, Rochester, NY) placed over the entrance aperture. As long as background light carried noise is the limiting noise, the S/N can be improved by using another filter with a narrower bandpass provided that the peak transmission of the filter is not reduced. However, the S/N for SEMIDS with a narrow filter can never be higher than that obtained by a colorimeter using the same filter if the whistle noise for SEMIDS is comparable to the drift noise for the colorimeter. If the same light gathering efficiency is assumed for both a colorimeter

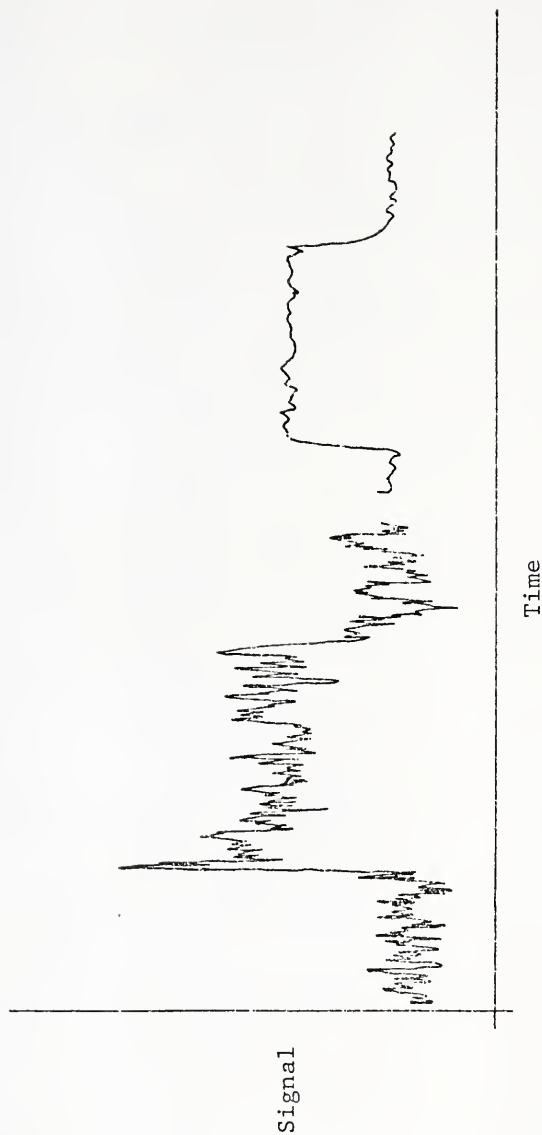


Figure 25. 589.0 nm Na flame emission for 0.1 ppm solution without (left trace) and with (right trace) a filter to limit the flame background emission.

and for SEMIDS plus the same filter, the signal throughput for the colorimeter will be greater by the factor 4 since no interference or modulation losses occur. If drift noise limits the colorimeter and whistle noise limits SEMIDS and if ξ_{db} for the colorimeter equals ξ_{wb} for SEMIDS, the colorimeter will have a higher S/N by the factor 2 because the factor S_1 will be close to unity over the narrow bandpass of the filter. If signal or background carried shot noise is the limiting noise, the colorimeter will be better by the factor $2\sqrt{2}$. Dominance by one of the signal carried proportional noises results in similar S/N for both instruments. Thus, the only advantage in using SEMIDS instead of a colorimeter is one of selectivity or resolution rather than S/N improvement.

Consideration of the equations in Table VIII leads to two possible applications where SEMIDS would provide a S/N improvement. First, any measurement which is limited by signal carried shot noise with absolutely no background present can be improved with SEMIDS. The S/N improvement factor will be $\sqrt{J/4}$ (as long as signal carried proportional noise remains negligible in SEMIDS). This factor is the Jacquinet advantage for shot noise limitation. Second, any measurement which is detector noise limited may be greatly improved by SEMIDS (if the same detector noise also limits SEMIDS). In this case, the S/N improvement factor will be $J/4$. This factor is the Jacquinet advantage for detector noise limitation.

CHAPTER VI CONCLUSIONS

The SEMIDS spectrometer can offer nearly a factor of 10^3 improvement in the luminosity-resolving power product as compared to a conventional spectrometer employing the same grating. However, this improvement can not lead to an improved S/N in any measurement which is not limited by detector noise where even a faint spectral background is present. Thus, in the uv-visible spectral region, all forms of absorption measurements must be eliminated from consideration as well as all sorts of flame and plasma measurements. A selectivity advantage is more likely to be achieved than a S/N advantage. Techniques already providing sufficient selectivity therefore could never be improved by using SEMIDS.

The only situation in the uv-visible spectral region where SEMIDS could offer S/N improvement is in the measurement of a sparse collection of faint narrow lines or bands requiring a high resolution measurement and with no background present. There is no analytical situation similar to this; however, some use might be found in astronomical spectrometry.

By far the most promising application of SEMIDS is for measurements in the infrared spectral region. The usual con-

dition of detector noise limitation would insure that the Jacquinot advantage would be realized in addition to a resolving power improvement. Therefore, SEMIDS should give performance intermediate to that of conventional infrared spectrometers and Fourier Transform Spectrometers (in which both the Jacquinot and the Fellgett advantage are realized). Because SEMIDS requires fewer components and requires much smaller mechanical tolerances (for example, no reference interferometer is required) as compared to the Fourier Transform Spectrometer, and also because no interferogram is produced thus eliminating the requirement of a computer or a Fourier Transform Analyzer, the cost of SEMIDS would be substantially lower than that of a Fourier Transform Spectrometer. Thus, SEMIDS could be a reasonable compromise for laboratories requiring an improved infrared spectrometer but without the budget for a Fourier Transform Spectrometer.

APPENDIX
DETERMINATION OF SHOT AND PROPORTIONAL COMPONENTS
OF OPTICAL NOISE

Optically carried noise can easily be characterized in terms of the shot and proportional noise components by a simple attenuation technique. Two noise measurements are required - one without and one with optical attenuation.

Let F be the attenuation factor ($1/T$) of a neutral density filter, N_{s1} and N_{p1} be the shot and proportional noises carried by the unattenuated light, respectively, and N_{s2} and N_{p2} be the shot and proportional noises carried by the attenuated light, respectively. The relations

$$\frac{N_{s1}}{\sqrt{F}} = N_{s2} \quad (A1)$$

and

$$\frac{N_{p1}}{F} = N_{p2} \quad (A2)$$

are established by the character of shot and proportional noise. Only total noises can be measured. The square of the total noise for the attenuated light is

$$N_{T2}^2 = N_{s2}^2 + N_{p2}^2 = \frac{N_{s1}^2}{F} + \frac{N_{p1}^2}{F^2} \quad (A3)$$

while that of the unattenuated light is

$$N_{T1}^2 = N_{s1}^2 + N_{p1}^2 . \quad (A4)$$

Rearranging yields

$$N_{p1}^2 = N_{T1}^2 - N_{s1}^2 . \quad (A5)$$

Substituting Equation A5 into Equation A3 and solving for N_{s1} results in

$$N_{s1} = \sqrt{\frac{F^2 N_{T2}^2 - N_{T1}^2}{F - 1}} . \quad (A6)$$

Substituting Equation A6 into Equation A5 and solving for N_{p1} results in

$$N_{p1} = \sqrt{\frac{F N_{T1}^2 - F^2 N_{T2}^2}{F - 1}} . \quad (A7)$$

Thus, the shot and proportional noise components of the unattenuated light can be found by two measurements of total noise.

LITERATURE CITED

1. A. A. Michelson, Light Waves and Their Uses, University of Chicago Press, Chicago, 1902.
2. M. Françon, Optical Interferometry, Academic Press, New York, 1966, pp. 87-91.
3. S. Tolansky, An Introduction to Interferometry, Longmans, Green and Co., Ltd., London, 1955, pp. 84-107.
4. M. Born and E. Wolf, Principles of Optics, Third (Revised) Edition, Pergamon Press, Oxford, 1965, pp. 300-303.
5. F. A. Jenkins and H. E. White, Fundamentals of Optics, Third Edition, McGraw-Hill Book Company, Inc., New York, 1957, pp. 244-256.
6. J. F. James and R. S. Sternberg, The Design of Optical Spectrometers, Chapman and Hall, Ltd., London, 1969, pp. 116-140.
7. A. P. Thorne, Spectrophysics, Chapman and Hall, Ltd., London, 1974, pp. 189-206.
8. R. N. Ibbett, D. Aspinall and J. R. Grainger, Appl. Opt. 7, 1089 (1968).
9. J. A. Decker and M. O. Harwit, Appl. Opt. 7, 2205 (1968).
10. E. D. Nelson and M. L. Fredman, J. Opt. Soc. Amer. 60, 1665 (1970).
11. F. W. Plankey, T. H. Glenn, L. P. Hart and J. D. Winefordner, Anal. Chem. 46, 1195 (1974).
12. L. Mertz, Transformations in Optics, John Wiley and Sons, Inc., New York, 1965, pp. 64-76.
13. A. Walsh, Atomic Absorption Conf., Sheffield, England, June, 1969.
14. T. L. Chester and J. D. Winefordner, Spectrochim. Acta 31B, 21 (1976).

15. T. Hirschfeld, 28th Annual Symposium on Analytical Chemistry: New Horizons in Analytical Spectroscopy, Knoxville, TN, June, 1975.
16. R. T. Weidner and R. L. Sells, Elementary Classical Physics, Vol. 2, Allyn and Bacon, Inc., Boston, 1965, p. 950.
17. W. H. Steel, Interferometry, Cambridge University Press, Cambridge, 1967, pp. 40-54.
18. A. P. Thorne, op. cit., pp. 172-189.
19. S. Tolansky, op. cit., pp. 128-143.
20. R. J. Bell, Introductory Fourier Transform Spectroscopy, Academic Press, New York, 1972, p. 149.
21. Ibid., p. 73.
22. Ibid., pp. 69-77.
23. R. B. Blackman and J. W. Tukey, The Measurement of Power Spectra, Dover Publications, Inc., New York, 1958.
24. P. Connes, J. Phys. Rad. 19, 197 (1958).
25. J. Meaburn, Appl. Opt. 14, 2521 (1975).
26. A. Girard, Appl. Opt. 2, 79 (1963).
27. J. Meaburn, Appl. Opt. 12, 2869 (1973).
28. J. Meaburn, Appl. Opt. 12, 279 (1973).
29. V. Arkhipov et al., Sov. J. Opt. Technol. 33, 545 (1966).
30. M. A. Gershun, Sov. J. Opt. Technol. 41, 559 (1974).
31. P. Connes, Opt. Acta 4, 136 (1957).
32. P. Connes, Rev. Opt. 39, 402 (1960).
33. P. Ramsey and T. Schroeder, J. Opt. Soc. Amer. 24, 353 (1959).
34. P. Ramsey and T. Schroeder, J. Opt. Soc. Amer. 30, 355 (1965).
35. A. Girard and P. Jacquinot, "Instrumental Methods," in Advanced Optical Techniques, A. C. S. Van Heel, Ed., John Wiley, New York, 1967.

36. P. Connes, Rev. Opt. 38, 157 (1959).
37. P. Jacquinot, Rept. Progr. Phys. 23, 267 (1960).
38. S. M. Till, W. J. Jones and K. C. Shotton, Proc. Roy. Soc. London A 346, 395 (1975).
39. J. Dupré, P. Pinson, C. Meyer and P. Barchewitz, Appl. Opt. 10, 1177 (1974).
40. P. Pinson, Appl. Opt. 13, 1618 (1974).
41. G. Grainer, J. Phys. 26, 222A (1965).
42. Handbook of Chemistry and Physics, 51st Edition, Chemical Rubber Company, Cleveland, Ohio, 1970, p. E-231.
43. T. Dohi and T. Suzuki, Appl. Opt. 10, 1359 (1971).
44. J. J. Fitzgerald, T. L. Chester and J. D. Winefordner, Anal. Chem. 47, 2330 (1975).
45. T. Suzuki and T. Dohi, Japan J. Appl. Phys. 14 (1975), Suppl. 14-1, p. 79.
46. "Molelectron Dye Laser Manual, DL-Series Tunable Dye Laser," Molelectron Corporation, Sunnyvale, California.
47. W. H. Steel, op. cit., p. 94.
48. P. Pinson and J. P. Guillotin, Rev. Phys. Appl. 7, 335 (1972).
49. H. V. Malmstadt, C. G. Enke, S. R. Crouch and G. Horlick, Optimization of Electronic Measurements, W. A. Benjamin, Inc., Menlo Park, California, 1974, pp. 66-67.
50. H. V. Malmstadt, C. G. Enke and S. R. Crouch, Control of Electrical Quantities, W. A. Benjamin, Inc., Menlo Park, California, 1974, pp. 237-239.
51. J. D. Winefordner, R. Avni, T. L. Chester, J. J. Fitzgerald, L. P. Hart, D. J. Johnson and F. W. Plankey, Spectrochim. Acta 31B, 1 (1976).
52. P. L. Larkins, R. M. Lowe, J. V. Sullivan and A. Walsh, Spectrochim. Acta 24B, 187 (1969).
53. P. L. Larkins, Spectrochim. Acta 26B, 477 (1971).
54. P. L. Larkins and J. B. Willis, Spectrochim. Acta 26B, 491 (1971).

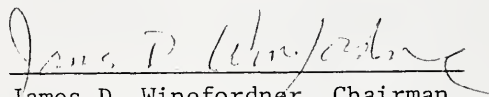
55. T. J. Vickers and R. M. Vaught, Anal. Chem. 41, 1476 (1969).
56. T. J. Vickers, P. Slevin, V. I. Muscat and L. T. Farias, Anal. Chem. 44, 930 (1972).
57. V. I. Muscat, T. J. Vickers, W. E. Rippetoe and E. R. Johnson, Appl. Spectrosc. 29, 52 (1975).
58. Y. I. Belyaev, L. M. Ivantsov, A. V. Karyakin, P. H. Phi and V. V. Shemet, J. Analyt. Chem. USSR 23, 855 (1968).
59. C. T. J. Alkemade, H. P. Hooymayers, P. L. Lijinse and T. J. M. J. Vierbergen, Spectrochim. Acta 27B, 149 (1972).
60. V. G. Mossotti and F. N. Abercrombie, Colloquium Spectroscopicum Internationale XVI, Heidelberg, Vol. II, Hilger, London, 1971.
61. T. C. O'Haver and C. P. Thomas, Pittsburgh Conference on Analytical Chemistry and Applied Spectroscopy, Cleveland, Ohio, March 1972.
62. G. V. Papayan and Y. M. Rozanov, J. Opt. Technol 36, 97 (1969).
63. V. G. Mossotti, Anal. Chem., in press.
64. G. M. Hieftje, Anal. Chem. 44, 81A (1972).
65. Y. Talmi, R. Crosmun and N. M. Larson, Anal. Chem. 48, 326 (1976).
66. G. M. Hieftje and R. I. Bystroff, Spectrochim. Acta 30B, 187 (1975).
67. A. S. Filler, J. Opt. Soc. Amer. 63, 589 (1973).
68. T. Hirschfeld, Appl. Spectrosc. 30, 68 (1976).
69. T. L. Chester, J. J. Fitzgerald and J. D. Winefordner, Anal. Chem. 48, 779 (1976).
70. D. J. Johnson, F. W. Plankey and J. D. Winefordner, Anal. Chem. 47, 1739 (1975).

BIOGRAPHICAL SKETCH

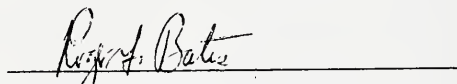
Thomas Lee Chester was born on September 28, 1949 in Jacksonville, Florida. He attended public schools in Jacksonville and graduated from Terry Parker Senior High School in 1967. That year, he enrolled in the Florida State University and graduated with the Bachelor of Science degree in June, 1971. He was employed by the Verona Division of the Baychem Corporation, Charleston, South Carolina, from July, 1971 to September, 1972, after which he began his graduate program at the University of Florida.

He married the former Ellen Watts Quigley on December 28, 1970. His daughter, Carolyn, was born on January 28, 1974.


I certify that I have read this study and that in my opinion it conforms to acceptable standards of scholarly presentation and is fully adequate, in scope and quality, as a dissertation for the degree of Doctor of Philosophy.


James D. Winefordner, Chairman
Professor of Chemistry

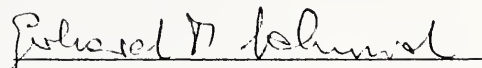
I certify that I have read this study and that in my opinion it conforms to acceptable standards of scholarly presentation and is fully adequate, in scope and quality, as a dissertation for the degree of Doctor of Philosophy.


Roger G. Bates
Professor of Chemistry

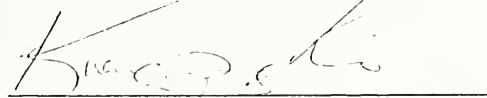
I certify that I have read this study and that in my opinion it conforms to acceptable standards of scholarly presentation and is fully adequate, in scope and quality, as a dissertation for the degree of Doctor of Philosophy.


John E. Singley
Professor of Environmental
Engineering Science

I certify that I have read this study and that in my opinion it conforms to acceptable standards of scholarly presentation and is fully adequate, in scope and quality, as a dissertation for the degree of Doctor of Philosophy.


Gerhard M. Schmid
Associate Professor of Chemistry

I certify that I have read this study and that in my opinion it conforms to acceptable standards of scholarly presentation and is fully adequate, in scope and quality, as a dissertation for the degree of Doctor of Philosophy.


Kuang-pang Li
Assistant Professor of Chemistry

This dissertation was submitted to the Graduate Faculty of the Department of Chemistry in the College of Arts and Sciences and to the Graduate Council, and was accepted as partial fulfillment of the requirements for the degree of Doctor of Philosophy.

June, 1976

Dean, Graduate School

